

Rasmus Møller Guttormsen

# Analytical Solutions and Advanced Software Simulation of Vibration Dampers

Master's thesis in Manufacturing Technology

Supervisor: Knut Sørby

Co-supervisor: Chao Gao

June 2023



Rasmus Møller Guttormsen

# **Analytical Solutions and Advanced Software Simulation of Vibration Dampers**

Master's thesis in Manufacturing Technology  
Supervisor: Knut Sørby  
Co-supervisor: Chao Gao  
June 2023

Norwegian University of Science and Technology  
Faculty of Engineering  
Department of Mechanical and Industrial Engineering





---

## Preface

This thesis, written in the spring of 2023, concludes my master's degree in Mechanical and Industrial engineering at the Norwegian University of Science and Technology. The thesis explores the behavior of a vibration damper through a comparative analysis between analytical solutions and advanced software. Problems that originate from vibrations are frequently encountered in boring when machining with long overhangs. Damped tools can solve vibration issues and improve boring performance.

I would like to extend a special thanks to my supervisor, Knut Sørby, for his guidance and patience throughout the time-consuming challenges encountered while working with Abaqus. Additionally, I am grateful to my co-supervisor, Chao Gao, for providing valuable assistance in overcoming technical obstacles related to the software. It has been an immensely interesting experience delving into this subject due to its relevance. The concept of a two-mass damping system is not only applicable to a boring bar but also finds relevance in various vibrations occurring around us. Exploring damping techniques and simulating them has been an enriching learning journey.

The rubber material, with its unique properties, holds exceptional potential and applicability in environments that require effective vibration damping. Its versatility and effectiveness make it a valuable asset.

Through this thesis, I aim to shed light on the aspects of vibration damping, analyze the capabilities of Abaqus, and explore the broader applications of damping techniques. It is my hope that this work will contribute to the growing interest in this field and inspire further research and advancements.



Rasmus Møller Guttormsen

Trondheim, June 11, 2023



---

## Abstract

This thesis focuses on three key aspects of damping phenomena: viscous fluid, spring/dashpot elements in Abaqus, and rubber elements. Fluid simulations are analyzed using a technique where a part can be converted into particles acting as a viscous oil. The spring/dashpot element, a feature in Abaqus, allows the observation of its effect on damping behavior. The rubber elements are specifically investigated for their shear stiffness and damping behavior. These subjects are examined through combined simulations, resulting in frequency response functions for a simplified boring bar in Abaqus. By measuring the boring bar's response to varying input frequencies, it provides information about its dynamic behavior. The findings demonstrate a close alignment between the analytical approach and the Abaqus model, particularly in terms of shear stiffness, which also matches the Matlab model.

The study also investigates the impact of viscous damping on a moving mass. Since Abaqus does not allow running a frequency response function directly by converting a part to particles, a workaround involves adding a periodic force to a cylindrical mass moving inside a container and interacting with fluid. Comparing three different scenarios, the results indicate that Abaqus demonstrates the effect of viscous damping for both the dashpot element and the smoothed particle hydrodynamics model.

Overall, this thesis provides valuable insights into the behavior of various damping elements and their impact on the frequency response of the boring bar. The comparative analyses between analytical and simulation approaches in Abaqus, along with the inclusion of viscous damping effects, contribute to a comprehensive understanding of damping phenomena.





---

## Sammendrag

Denne masteroppgaven fokuserer på tre sentrale aspekter ved dempingsfenomener: viskøs væske, fjær/dempererlementer i Abaqus og gummi-elementer. Væske-simuleringer analyseres ved hjelp av en teknikk der et objekt kan konverteres til partikler som oppfører seg som en viskøs olje. Fjær/dempererlementet, en funksjon i Abaqus, tillater observasjon av dets påvirkning på dempingsoppførselen. Gummi-elementene undersøkes spesifikt med tanke på deres skjærstivhet og dempingsoppførsel. Disse emnene blir undersøkt gjennom kombinerte simuleringer, som resulterer i frekvensresponsfunksjoner for en forenklet verktøyholder i Abaqus. Ved å måle verktøyholderens respons på varierende frekvenser gir det informasjon om dens dynamiske oppførsel. Resultatene viser en tett sammenheng mellom den analytiske tilnærmingen og Abaqus-modellen, spesielt med hensyn til skjærstivhet, som også matcher Matlab-modellen.

Studien undersøker også virkningen av viskøs demping på en bevegelig masse. Siden Abaqus ikke tillater direkte simulering av en frekvensresponsfunksjon ved å konvertere et objekt til partikler, er metoden for å oppdage demping å legge til en periodisk kraft til en sylindrisk masse som beveger seg inne i en beholder og omgitt av viskøs væske. Sammenligning av tre forskjellige scenarier viser at Abaqus demonstrerer virkningen av viskøs demping både for fjær/dempererlementet og ved bruk av "smoothed particle hydrodynamics" teknikken.

Alt i alt gir denne oppgaven verdifulle innsikter i oppførselen til ulike dempingselementer og deres innvirkning på frekvensresponsen til verktøyholderen. De sammenlignende analysene mellom analytiske og simulerte tilnærminger i Abaqus, samt inkluderingen av viskøs dempingseffekter, bidrar til en helhetlig forståelse av dempingsfenomener.



---

# Table of Contents

<b>List of Figures</b>	<b>viii</b>
<b>List of Tables</b>	<b>x</b>
<b>1 Introduction</b>	<b>1</b>
1.1 Objective . . . . .	1
1.2 Method . . . . .	1
<b>2 Theoretical Background</b>	<b>2</b>
2.1 Viscosity . . . . .	2
2.1.1 Viscous Damping Elements . . . . .	3
2.1.2 Terminal Velocity . . . . .	3
2.1.3 Reynolds Number . . . . .	4
2.2 Fluid-Structure Interaction . . . . .	5
2.2.1 Smoothed Particle Hydrodynamics . . . . .	6
2.3 Dynamic Analysis in FEM . . . . .	6
2.4 Abaqus Features . . . . .	8
2.4.1 Spring/dashpot Elements in Abaqus . . . . .	8
2.4.2 Amplitude Definition . . . . .	8
2.5 Rayleigh Damping Coefficients . . . . .	9
<b>3 Validation of Fluid Simulations</b>	<b>12</b>
3.1 Translatory Coefficient of Viscous Damping . . . . .	12
3.2 Rotary Coefficient of Viscous Damping . . . . .	15
3.3 Fluid Simulations Summary . . . . .	18
<b>4 Spring/Dashpot in Abaqus</b>	<b>19</b>
4.1 Experimental Spring/Dashpot Testing . . . . .	19
4.2 Verify Dashpot Element . . . . .	23
4.3 Spring/Dashpot Summary . . . . .	25
<b>5 Rubber Testing and Simulating</b>	<b>26</b>
5.1 Damping Consideration and Impact Simulation . . . . .	26
5.2 Rubber Element Shear Stiffness . . . . .	28
5.3 Rubber Element Summary . . . . .	30
<b>6 Combined Simulations</b>	<b>31</b>

---

6.1	Tuned Mass Damper Simulation . . . . .	31
6.2	A Fluid-Affected Mass Subjected to Periodic Force . . . . .	35
<b>7</b>	<b>Discussion</b>	<b>38</b>
7.1	Assessment of Shear Stiffness . . . . .	38
7.2	Evaluation of Fluid Simulations . . . . .	39
<b>8</b>	<b>Conclusion</b>	<b>41</b>
8.1	Further Work . . . . .	41
	<b>Bibliography</b>	<b>43</b>
	<b>Appendix</b>	<b>45</b>
A	Rotary Damping Data . . . . .	45
B	Abaqus Meshing Techniques . . . . .	46
C	Optimal TMD Matlab Code . . . . .	48

## List of Figures

1	Centipoise Vs. Centistoke . . . . .	2
2	Fluid Relative Motion . . . . .	3
3	Creeping Flow Past a Sphere . . . . .	4
4	Drag Coefficient and Reynolds Number . . . . .	5
5	SPH Particle Distribution . . . . .	6
6	Implicit Solver and Explicit Solver . . . . .	7
7	Amplitude in Abaqus - Define . . . . .	9
8	Amplitude in Abaqus - Periodic . . . . .	9
9	Half Power Bandwidth Method . . . . .	10
10	Mobile Cylinder Falling Through Fluid . . . . .	12
11	The Iterated Approach Calculation . . . . .	13
12	SPH Start Position . . . . .	14
13	SPH End Position . . . . .	14
14	Velocity-Time SPH Data . . . . .	14
15	Theoretical Journal Bearing . . . . .	15
16	View Cut of Rotary Model . . . . .	16
17	Rotary Motion . . . . .	17
18	Torque-Tangential Speed Plot . . . . .	18

---

19	Model with Spring/dashpot . . . . .	19
20	Spring Plot . . . . .	20
21	Spring/dashpot Plot . . . . .	20
22	Square Bar Static Deflection Analysis . . . . .	21
23	Square Bar Eigenvalues . . . . .	21
24	Rayleigh Damping Coefficient of the Bar . . . . .	22
25	Rayleigh Coefficient Input . . . . .	22
26	Damper/Dashpot Input Parameters . . . . .	22
27	Simplified 2DOF FRF plot comparison . . . . .	23
28	Damped lumped parameter model . . . . .	24
29	Dashpot in 1DOF Model . . . . .	24
30	Mode frequencies . . . . .	26
31	Rayleigh damping coefficients . . . . .	27
32	Time-domain Attenuation Curves . . . . .	27
33	Boundary Conditions Rubber Element . . . . .	28
34	Deflection Result . . . . .	29
35	Shear Stiffness 1 Vs 2 rubber elements . . . . .	29
36	Boundary Conditions of Tool . . . . .	32
37	Tool Geometry With Integrated Damper at the Tip . . . . .	32
38	Static Deflection Analysis . . . . .	33
39	Tool Body Eigenvalues . . . . .	33
40	Frequency Response Function without Damper . . . . .	34
41	FRF Plot Comparison . . . . .	34
42	Adjusted FRF Plot Comparison . . . . .	35
43	A View-Cut of The Fluid-Affected Mass Model . . . . .	36
44	Periodic Force ( $\sin(10\pi)$ ) Vs Mass Displacement . . . . .	36
45	Periodic Force ( $\sin(5\pi)$ ) Vs Mass Displacement . . . . .	37
46	Rotary motion from SPH simulations . . . . .	45
47	Tool Mesh . . . . .	46
48	Rubber Element Mesh . . . . .	46
49	Dampening Mass Mesh . . . . .	46
50	Fluid Mesh . . . . .	47
51	Conversion To Particles . . . . .	47

---

## List of Tables

1	Translatory model material data . . . . .	12
2	Rotary model material data . . . . .	15
3	Material properties for steel, rubber, and fluid . . . . .	31
4	Rotary model results . . . . .	45

## Symbols

$F_d, f_d$  - Translatory dampening force, as for viscous resistance  
 $c_t$  - Translatory damping coefficient  
 $m_d$  - Rotation damping moment  
 $c_r$  - Rotary damping coefficient  
 $\tau$  - Shear stress  
 $\mu$  - Dynamic viscosity  
 $C_d$  - Drag coefficient  
 $\rho$  - Density  
 $v$  - Velocity  
 $A$  - Projected area  
 $m$  - Mass  
 $g$  - Gravity  
 $Re$  - Reynolds number  
 $D, d$  - Diameter  
 $t$  - Time  
 $C$  - System damping matrix  
 $M$  - System structural mass matrix  
 $K$  - System structural stiffness matrix  
 $\alpha$  - Rayleigh damping coefficient proportional to the mass of the system  
 $\beta$  - Rayleigh damping coefficient proportional to the stiffness of the system  
 $\xi$  - Damping ratio  
 $f_n, \omega$  - Frequency  
 $x$  - Deflection

---

# 1 Introduction

The present master's thesis focuses on investigating damping phenomena within the Abaqus software. The study examines the damping effects of both an elastic rubber material and a viscous liquid modeled as particles. The damping phenomena are analyzed using a two-mass system, which is a system used in the Silent Tool (boring bar), developed by Sandvik Coromant. In contrast to shorter cutting tools, a boring bar is characterized by its elongated structure. This design makes it prone to vibrations when delivering cutting forces.

The experimental setup is based on the Silent Tool. The Silent Tool utilizes a damping technique called tuned mass damping, wherein a counterweight within the tool absorbs kinetic energy from vibrations. By employing a compensating frequency, these vibrations are mechanically eliminated. The tuned mass damper plays a crucial role in mitigating uncontrolled vibrations in machining tools. The target of this research is to assess the capability of finite element analysis software in accurately simulating the vibration behavior of a simplified Silent Tool.

The research process involves conducting experiments using the rubber material to simulate spring and the oil to mimic the dampening effect within Abaqus. Both static and dynamic analyses are performed to investigate parameters such as shear stiffness, impact deflection, frequency response function, and smoothed particle hydrodynamic analysis.

## 1.1 Objective

The main goal of this master's thesis is to confirm that Abaqus can produce accurate and dependable results. Validating Abaqus will allow Sandvik Coromant to make adjustments to tool designs or material properties more efficiently. This, in turn, will enable the company to save time and money by conducting cost-effective experiments on specific parts of the Silent Tool. For example, they can explore different geometries or material properties for the rubber element and experiment with various viscous fluids by adjusting the viscosity to achieve different damping effects.

To achieve these objectives, the plan is to establish clear and measurable outcomes by following a systematic process. The first steps involve becoming familiar with the relevant field of study and further building on the knowledge of damping in a two-mass system. This knowledge will guide the appropriate analyses to be conducted in Abaqus and determine a proper approach for implementing them. However, it is important to acknowledge that certain assumptions need to be made to accommodate limitations and simplify the experimental setup.

## 1.2 Method

By comparing results obtained from Abaqus with analytical calculations in Matlab, a fundamental understanding of the system can be established. The analytical approach in Matlab relies on theoretical formulas.

Abaqus is a finite element analysis software program that provides a range of simulation capabilities. These simulations encompass simple static analyses with uniaxial stress loads, as well as frequency and steady-state dynamic analyses. Additionally, Abaqus extends its scope to include fluid-structure interaction simulations using the smoothed particle hydrodynamics method.

The analytical calculations are based on the modal analysis theory described in the book "Machining Dynamics" by Tony L. Schmitz and Kevin S. Smith. For the theoretical calculations concerning viscous damping elements, the book "System Dynamics for Engineering Students" by Nicolae Lobontiu is referenced.

Matlab is chosen for this project specifically because of its robust "fminsearch" function, which greatly enhances the capabilities of running optimized frequency response functions. Matlab is a high-level programming language and environment designed for numerical computation, visualization, and data analysis.

---

## 2 Theoretical Background

The theoretical background section provides a foundation for the results presented in the master thesis. It covers several key subjects that directly and indirectly contribute to the findings.

Firstly, fluid mechanics is explored as a branch of physics that investigates the properties and behavior of fluids under external forces. Viscosity, a fundamental property in fluid mechanics, is discussed in relation to a fluid's resistance to flow. Its significance in practical applications is emphasized.

The section delves into different types of viscous damping elements resulting from fluid viscosity. Both translatory and rotary damping elements are explained. Additionally, the concept of terminal velocity, which represents the equilibrium between gravitational and drag forces when an object falls through a fluid, is highlighted.

The two dynamic analysis methods offered by Abaqus and their respective applications are elaborated. It also examines the concept of fluid-structure interaction, which involves studying the interaction between a fluid and a solid structure. Furthermore, the smoothed particle hydrodynamics approach, a commonly used numerical method for simulating fluid-structure interaction problems, is discussed in detail. Additionally, two notable features in Abaqus, namely the spring/dashpot element and the amplitude feature, are explored.

Lastly, the Rayleigh damping coefficient is elaborated. The half-power bandwidth method is employed to estimate the required damping ratio, which is essential for calculating the damping coefficients  $\alpha$  and  $\beta$ .

### 2.1 Viscosity

When studying fluid flow for any purpose, viscosity becomes a fundamental material property that needs to be considered. Viscosity can take on two primary forms: dynamic and kinematic. This subsection will explain their differences.

Dynamic viscosity, also known as absolute viscosity, is a measure of a fluid's internal resistance to flow. Kinematic viscosity, on the other hand, is the ratio of dynamic viscosity to density. It is important to note that two fluids with the same dynamic viscosity can have different kinematic viscosity depending on their density. Put simply, dynamic viscosity provides information on the force required to make the fluid flow through a tube illustrated as (a) in Figure 1. While (b) shows that kinematic viscosity refers to the timed flow rates through orifices, usually driven by the force of gravity.[1]

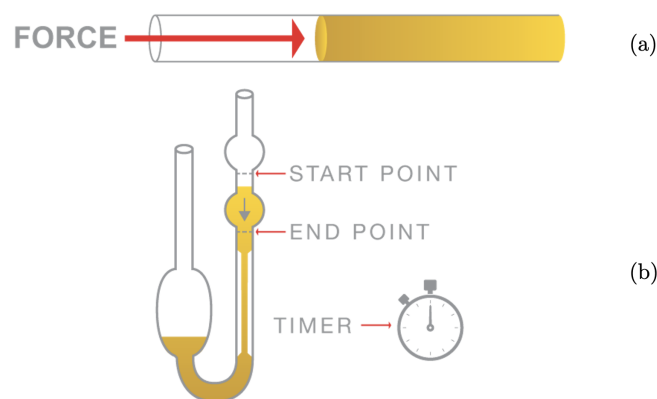


Figure 1: (a); The force required to overcome fluid resistance to flow through a tube. (b); Timed flow rates through orifices.

Source: [2]



The variety of viscosity units can appear extensive. The dimensions of dynamic viscosity are  $force \times time \div area$ . Where the unit is Newton-second per square meter, and can also be expressed as pascal-second in SI units.  $1 \text{Ns/m}^2 = 1 \text{kg}/(\text{m}\cdot\text{s}) = 1 \text{Pa}\cdot\text{s} = 10 \text{P}$  where the unit poise (P) is often used with the metric prefix centipoise because the viscosity of water at  $20^\circ\text{C}$  is 1 centipoise. Kinematic viscosity is obtained by dividing the dynamic viscosity of a fluid by its mass density. The dimensions of kinematic viscosity are  $area \div time$ , and the appropriate units of measurement are meters squared per second. In the centimeter-gram-second system, the unit of kinematic viscosity is called stokes (sT). The stoke is defined as one centimeter squared per second.  $1 \text{sT} = 1 \text{cm}^2/\text{s} = 0.0001 \text{m}^2/\text{s}$ . [3]

### 2.1.1 Viscous Damping Elements

Damping is associated with energy losses, and in that regard, this section elaborates on studying viscous-type losses in relation to basic viscous dampers. In viscous damping, the damping force/torque is proportional to the relative velocity. Relative velocity refers to the velocity of an object with respect to the fluid. In other words, it is the difference between the velocity of the object and the velocity of the fluid. [4]

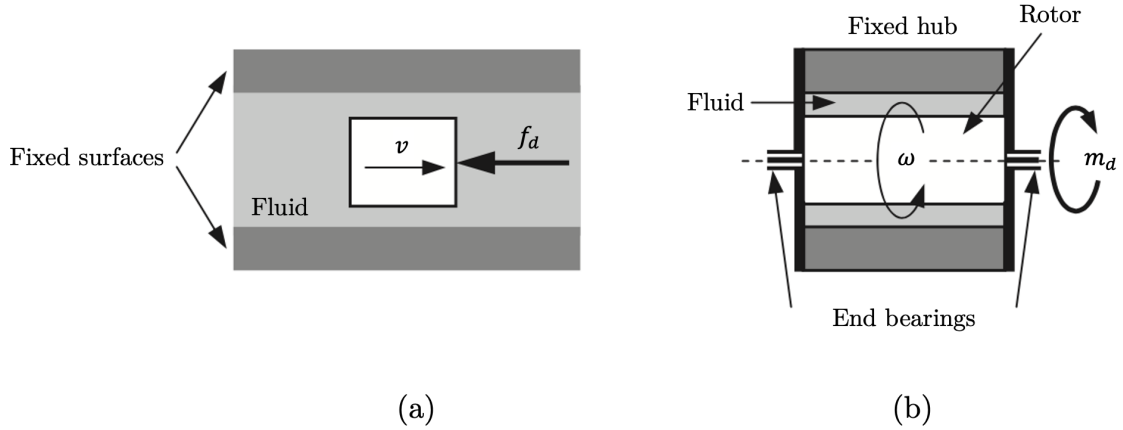


Figure 2: Damping through structure. (a); Translatory. (b); Rotary.

Source: [5]

Figure 2 illustrates the principle of translatory and rotary viscous damping. For translatory damping, a force ( $f_d$ ) is the viscous resistance. As for the force generated in rotary damping ( $m_d$ ) is the moment. This relationship is described by constant damping coefficients. The translatory damping force is expressed as  $f_d = c_t \cdot v(t)$  where  $c_t$  is the damping coefficient for translation. The rotation damping moment is written as  $m_d = c_r \cdot \omega(t)$  where  $c_r$  is the damping coefficient for rotation. These two viscous damping coefficients can be determined as a function of geometrical and material parameters. Newton's law of viscous flow is used, where it is established that shear stresses ( $\tau$ ) are created between adjacent fluid layers in both situations. If two surfaces move parallel to each other with fluid in between, the established shear stress is  $\tau = \mu \cdot dv(z)/dz$ . The coefficient of dynamic viscosity is represented as  $\mu$ , and  $dv(z)/dz$  is the gradient of the relative velocity. [5]

### 2.1.2 Terminal Velocity

The previous section is focusing on the linear profile of velocity between two close parallel surfaces. The attention in this section is about an object traveling through a fluid. The forces in focus are two external forces: the gravitational force, which is equivalent to its weight, and the resistance/drag force. If the object's mass stays constant, its movement can be explained using Newton's second law of motion, which states that force ( $F_g$ ) equals mass ( $m$ ) multiplied by acceleration ( $a$ ). The net external force ( $F$ ) is the difference between the gravitational and drag forces ( $F = F_g - F_d$ ). The

magnitude of the drag is given by the drag equation. Drag ( $F_d$ ) depends on the drag coefficient ( $C_d$ ), fluid density ( $\rho$ ), square of the fluid velocity ( $v$ ), and the projected area ( $A$ ) of the object used in Equation (1).[6]

$$F_d = \frac{1}{2}\rho v^2 C_d A \quad (1)$$

When the weight of an object is light, the point where the drag force equals the weight is quickly reached. At this point, the object experiences no net external force, and the vertical acceleration becomes zero. According to Newton's first law of motion, in the absence of any acceleration ( $F_d = F_g$ ), the object falls at a constant speed, as shown in Figure 3. Combining these two equations gives the terminal velocity Equation. (2).

$$v_{terminal} = \sqrt{\frac{2mg}{\rho C_d A}} \quad (2)$$

The geometrical shape, velocity, density, and viscosity of the fluid all affect the drag force. For instance, two objects with similar weight experience the same conditions, a streamlined body shape has a 0.04 drag coefficient enabling it to reach a higher terminal velocity than an object like a short cylinder shape with a 1.15 drag coefficient. An object's terminal velocity in water is lower than in air due to water's higher density.[7]

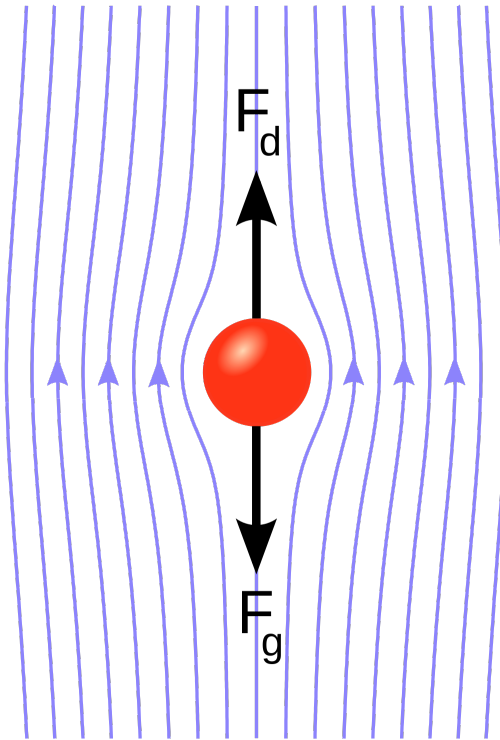


Figure 3: Creeping flow past a sphere: Drag force  $F_d$  and gravity  $F_g$ .

Source: [8]

### 2.1.3 Reynolds Number

The dimensionless Reynolds number ( $Re$ ) predicts whether the fluid flow would be laminar or turbulent. Laminar flow occurs at low  $Re$ , where viscous forces dominate and gives smooth fluid motions. When  $Re$  is high, the forces are dominated by inertial forces and result in turbulent flow,

hence the definition  $Re = \text{inertiaforce}/\text{viscousforce}$ . The properties affecting the prediction are the velocity, length, viscosity, and type of flow.[9]

When it comes to objects moving in a fluid, Reynolds number is called the particle Reynolds number  $Re_p$ , dependent on the surrounding flow and its fall velocity. The equation for the Reynolds number is represented as  $Re_p = \rho v d / \mu$ , where  $\rho$  is the fluid density,  $v$  is the relative velocity,  $d$  is the diameter for objects with the circular projected area and  $\mu$  is the dynamic viscosity. With a high viscosity, the flow is normally laminar and results in low  $Re$ . [10]

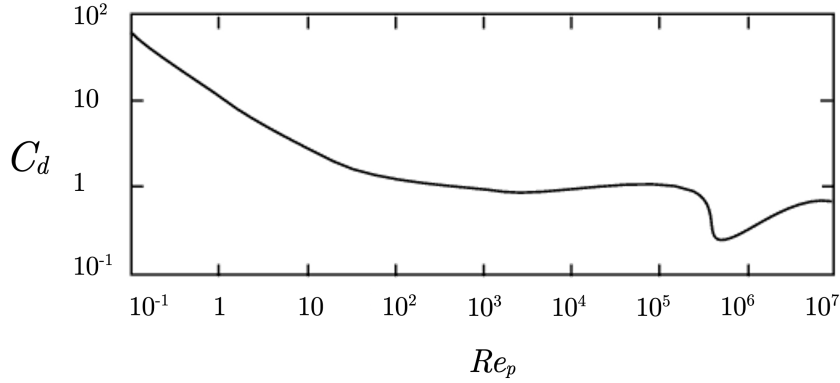


Figure 4: Correlation between drag coefficient  $C_d$  and Reynolds number  $Re_p$  for a cylinder

Source: [11]

An object's resistance or drag in a fluid environment is measured using the drag coefficient, and it correlates with Reynolds number as seen in Figure 4. The drag coefficient of a short cylinder when  $Re$  is  $0.1 \leq Re < 1000$ , can be calculated as  $C_d = 24/Re(1 + 0.15Re^{2/3})$ . [12]

## 2.2 Fluid-Structure Interaction

Fluid-structure interaction (FSI) refers to the analysis and simulation of the interaction between fluids and deformable structures. In Abaqus, FSI problems are solved by combining finite element method (FEM) for structural analysis and computational fluid dynamics (CFD) for fluid analysis. [13]

In the FEM approach of FSI, the structure is modeled using finite elements, and the governing equations for structural mechanics are solved. Instead of directly modeling the fluid, the fluid loads on the structure, such as pressure or drag forces, are obtained from CFD analysis. These fluid loads are then applied as boundary conditions on the structure, influencing its deformation and response. [14]

In the CFD approach of FSI, the focus is on modeling and solving the governing equations of fluid flow. The fluid domain is divided into small elements using a computational mesh, and the equations related to fluid dynamics are solved to determine the characteristics of fluid flow. The deformation of the structure is considered a boundary condition in the fluid domain, which in turn influences the patterns and properties of the fluid flow. [15]

The modeling approach in FSI can vary depending on the level of interaction between the fluid and structure, as well as the desired accuracy. For simpler FSI analyses that involve rigid body motion and heat transfer between the fluid and solid, a CFD approach can be used. In these cases, the solid component being studied typically does not undergo significant deformation or changes in shape. [16]

---

### 2.2.1 Smoothed Particle Hydrodynamics

Smoothed Particle Hydrodynamics is a method for simulating fluid flows and FSI problems. SPH has seen rapid development in the last decade due to its application to engineering problems for both fluids and solids.

SPH belongs to the meshless numerical methods family. Unlike Finite Element Analysis, these methods don't require defining nodes and elements. SPH relies on a collection of points that represent the body instead. These nodes are usually called particles and they are smoothed using a kernel function that assigns each particle a density and allows for interpolation of fluid properties such as pressure and velocity. However, it is important to note that SPH analysis can be computationally intensive and may require significant computational resources, particularly for large-scale problems.[17]

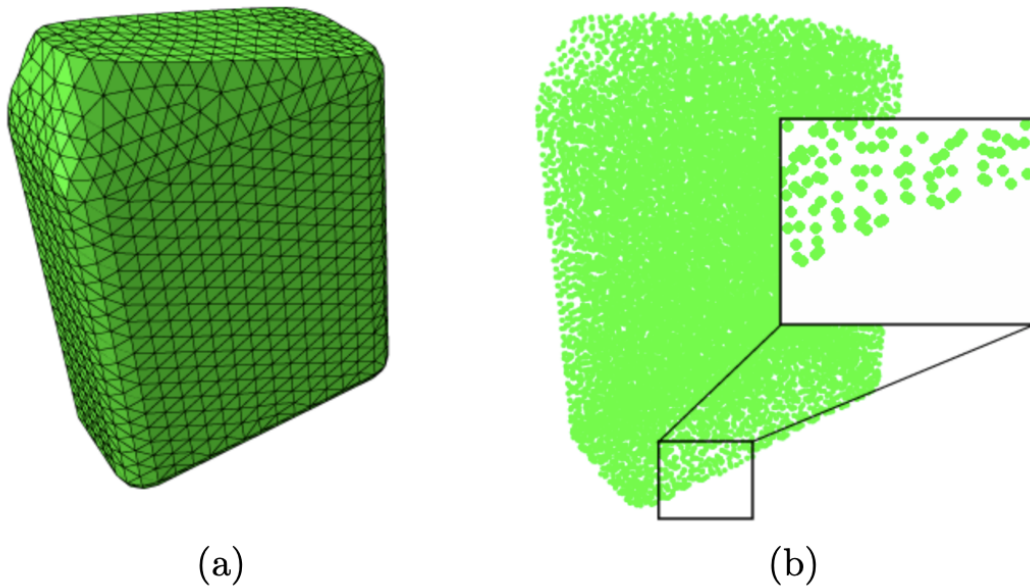


Figure 5: (a); Finite element mesh. (b); SPH particle distribution.

Source: [18]

The SPH method is particularly useful for simulating problems with large deformations or complex geometries, such as fluid flows around moving objects. To use the SPH method in Abaqus, the particle properties must be defined with material properties and initial position. The simulation parameters also need to be determined, such as the time step and the kernel function. The material density, dynamic viscosity, and equation of state (EOS) are required to achieve good accuracy in the analysis. The viscosity option is used in conjunction with the EOS option to accurately model fluid behavior in simulations. The combination of these two options allows for a more comprehensive representation of fluid dynamics and viscosity effects. The "Us-Up" type is a specific type of EOS that describes an isotropic compressible material with a linear relationship between the pressure and the volume change. When selecting "Us-Up" in "step 2" of defining the EOS behavior,  $c_0$  is the reference speed of sound. If EOS is not utilized in the simulation, it will lack essential information and eventually encounter errors, leading to termination. Abaqus provides a warning message stating that the viscosity option must be used in combination with the EOS option.[18]

### 2.3 Dynamic Analysis in FEM

Dynamic analysis in Abaqus refers to the simulation of the time-dependent behavior of a system under external loads. Unlike static analysis, dynamic analysis considers nodal forces associated

with mass/inertia and damping. Abaqus provides two numerical methods for dynamic analysis: the explicit solver and the implicit solver.[19]

Explicit dynamic analysis is a numerical method that solves the equations of motion using an explicit time integration scheme. This method is more accurate and efficient for simulations involving large deformations and strains, nonlinear material behavior, complex contact, and nonlinear buckling, seen in Figure 6 (b). The explicit solver is well-suited for smoothed particle hydrodynamics analysis because it can handle large deformations and high strain rates, which are common in fluid-structure interaction problems. The explicit solver is ideal for fast events and calculates the appropriate time increment based on the mesh, Young's modulus, density, and mass scaling. It is computationally efficient for large models with short dynamic response time and requires less computer storage as illustrated in Figure 6 (a).[20]

The implicit dynamic analysis uses an iterative approach to solve the equations of motion and is suitable for nonlinear problems that require solutions over multiple steps based on the previous solution. The implicit solver is recommended for structure dynamic types that involve applied displacements, low-frequency response, vibration, and oscillation. It is extremely time-consuming for large models and requires more computer storage. The primary distinction between implicit and explicit methods in numerical analysis is the manner in which they handle time incrementation, leading to differences in computational efficiency, accuracy, and applicability to different types of problems.[21]

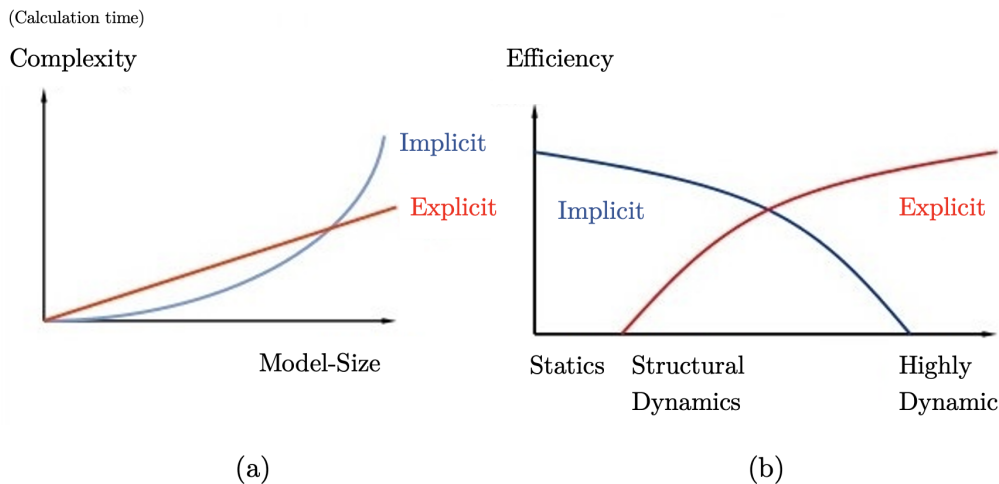


Figure 6: Solver comparison. (a); Computational cost-model size. (b); Efficiency-amount movement of an object.

Source: [22]

In dynamic analysis, the natural time scale is crucial, and it is essential to accurately represent the physical mass and inertia in the model to capture transient responses. However, there are often small elements that need to be included. These small elements pose a challenge for Abaqus, as it needs to accurately integrate the entire model over time. To achieve this accuracy, Abaqus uses small time increments during the simulation. The inclusion of small elements in the model is typically a consequence of difficulties encountered in generating the mesh, which is the process of dividing the model into smaller elements for analysis.[23]

One approach is to scale the masses of these elements. Mass scaling is a technique used to improve the efficiency and stability of simulations. It involves artificially increasing or decreasing the mass of the particles or elements in the model while preserving the overall behavior of the system. Mass scaling is a technique in SPH where particle masses are adjusted to achieve stability, accuracy, and computational efficiency. While it can reduce computational time, it may introduce errors

---

in the simulation. Mass scaling used in SPH analyses modifies the mass distribution of particles, potentially distorting the fluid flow behavior and leading to unrealistic fluid dynamics.[24]

## 2.4 Abaqus Features

This subsection discusses the dashpot and spring elements, their respective functions, and how they are used in modeling structures and materials. Further explains the significance of amplitude in Abaqus for dynamic analysis, where a periodic amplitude type is explained.

### 2.4.1 Spring/dashpot Elements in Abaqus

In Abaqus, dashpot and spring elements are used to model the viscoelastic behavior of materials. A dashpot element, also known as a viscous damper, is a component that provides resistance to motion through the action of a fluid. It consists of a piston moving within a cylinder filled with fluid. The fluid resistance is proportional to the velocity of the piston, creating a force that opposes motion. Dashpot elements are used to model damping in structures and materials.[25]

A spring element, on the other hand, is a component that resists deformation when a force is applied to it. It stores energy as it is deformed and releases it when the force is removed. Spring elements can be used to model the elastic behavior of materials and structures.[26]

In Abaqus, these elements can be used in combination to model viscoelastic materials, which exhibit both viscous and elastic behavior. Including both dashpot and spring elements in a model, makes it possible to simulate the time-dependent response of materials to mechanical loads. This is an important simulating feature that is used in many engineering applications where a model experience dynamic loading.[27]

### 2.4.2 Amplitude Definition

To perform dynamic analysis it is important to be familiar with the use of "Amplitude" in Abaqus. The amplitude option is used to specify a function that defines arbitrary time variations of prescribed variables throughout an analysis. There are multiple options for different types of amplitudes in Abaqus. Some of them are tabular, equally spaced, periodic, and modulated. In this project, the type of amplitude that is of particular relevance is the periodic amplitude. This type of amplitude refers to loads that repeat their motion within a specific time period. Equation (3) is the function to define the period amplitude.[28]

$$a = A_0 + \sum_{n=1}^N (A_n \cos n\omega(t - t_0) + B_n \sin n\omega(t - t_0)) \quad (3)$$

This function applies when  $t \geq t_0$ , for  $t < t_0$  then  $a = A_0$ . For example, if a sinus curve is desired,  $a = B_n \sin n\omega(t - t_0)$ , it can be plotted as illustrated in Figure 7.

The circular frequency, starting time, initial amplitude, and amplitudes  $A_n$  and  $B_n$  are the parameters required to define a periodic curve. Setting the circular frequency to  $2\pi$  determines that one wavelength corresponds to a duration of 1 second. The starting time dictates when the periodic amplitude initiates. The amplitude will remain its initial amplitude for as long  $t < t_0$ , the amplitude ( $a$ ) equals the initial amplitude ( $A_0$ ). In this particular example, the initial amplitude is -1 and remains constant for a duration of 0.25 seconds. The sinusoidal curve maintains a consistent amplitude ( $B_n$ ) of 2, as specified.

✚ Edit Amplitude
✕

Name: Sinus

Type: Periodic

---

Time Span:

Circular frequency:

Starting time:

Initial amplitude:

	A	B
1	0	2

Figure 7: Input parameters defining the periodic curve.

Figure 8 illustrates the sinusoidal curve that is obtained when plotting the input parameters shown in Figure 7. This example demonstrates how a load or displacement can be defined to change over time. By assigning a periodic amplitude to a force, for instance, the force will vary as time progresses.

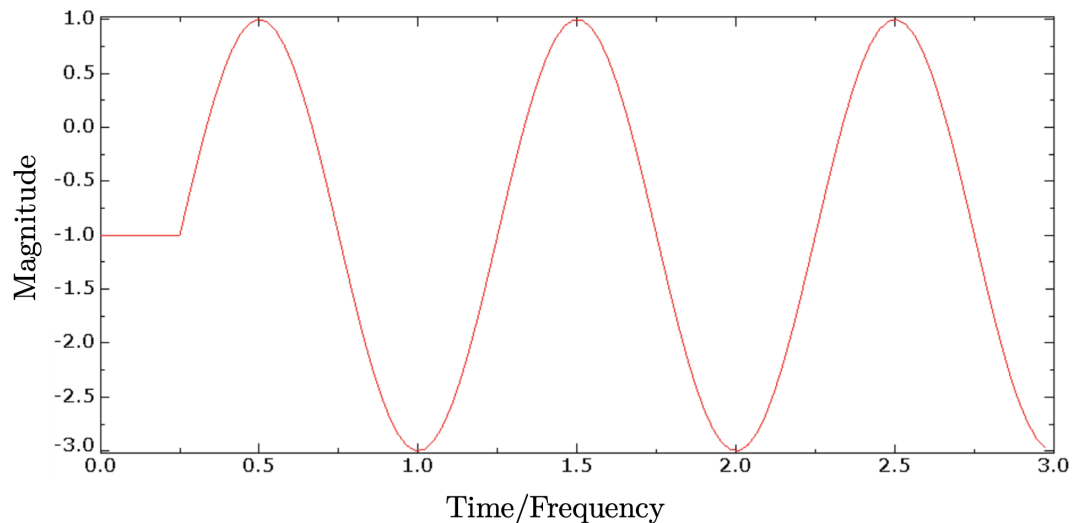


Figure 8: Periodic amplitude curve with given properties from Figure 7.

## 2.5 Rayleigh Damping Coefficients

The Rayleigh method is a suited approach to estimate the damping of a structure. It assumes that the damping can be represented by a linear combination of mass and stiffness matrices, with damping coefficients that are determined from a damping ratio and natural frequencies of the system. [29]

Rubber is a frequently utilized material in engineering applications for its capacity to provide damping in structures, effectively absorbing energy and diminishing vibrations. The damping characteristics of rubber are influenced by various factors, including the type of rubber, temper-

ature, and vibration frequency. When employing the Rayleigh method on a structure containing damping rubber, the initial step involves estimating the system's natural frequencies. This estimation can be achieved through finite element analysis or experimental modal analysis. Once the natural frequencies are determined, the damping ratio can be calculated, and the damping matrix is expressed through Equation (4).[30]

$$[C] = \alpha[M] + \beta[K] \quad (4)$$

$[C]$  is the system damping matrix,  $[M]$  is the system structural mass matrix,  $[K]$  is the system structural stiffness matrix. The coefficient  $\alpha$  represents the Rayleigh damping that is proportional to the mass of the system, while the coefficient  $\beta$  represents the damping that is proportional to the stiffness of the system.[31]

The Rayleigh method is used to determine the damping coefficients  $\alpha$  and  $\beta$ . The two specific natural frequency of the modes is  $\omega_1$  and  $\omega_2$ . The damping ratio associated with  $\omega_1$  and  $\omega_2$  is  $\xi_1$  and  $\xi_2$ . The relations between them can be expressed in the following equation.

$$\begin{Bmatrix} \alpha \\ \beta \end{Bmatrix} = 2 \frac{\omega_1 \omega_2}{\omega_2^2 - \omega_1^2} \begin{bmatrix} \omega_2 & -\omega_1 \\ -\omega_2^{-1} & \omega_1^{-1} \end{bmatrix} \begin{Bmatrix} \xi_1 \\ \xi_2 \end{Bmatrix} \quad (5)$$

Equation (5) can be simplified by assuming that the same damping ratio is applied to both  $\omega_1$  and  $\omega_2$  in real practice.

$$\begin{Bmatrix} \alpha \\ \beta \end{Bmatrix} = \frac{2\xi}{\omega_1 + \omega_2} \begin{Bmatrix} \omega_1 \omega_2 \\ 1 \end{Bmatrix} \quad (6)$$

The damping ratio ( $\xi$ ) can be obtained experimentally using various testing methods. The damping ratio of rubber can be determined using the half-power bandwidth method. The half-power bandwidth method is a technique used to determine the damping ratio of a mechanical or structural system from its frequency response function. This method involves calculating the difference between the frequencies  $f_1$  and  $f_2$ , which is known as the bandwidth illustrated in Figure 9. To determine these frequencies, one can locate the corresponding position of  $A_{max}/\sqrt{2}$ , where  $A_{max}$  represents the peak amplitude.[32]

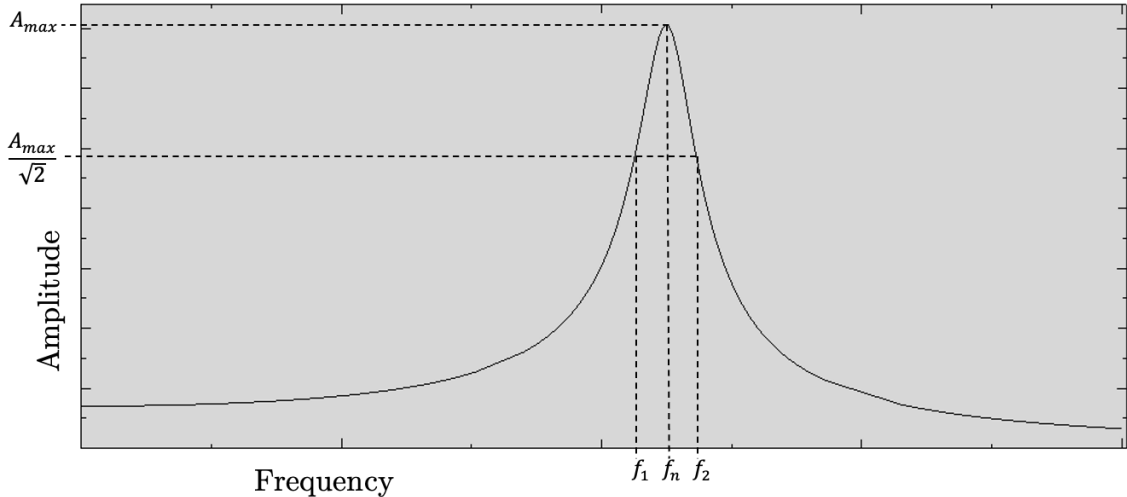


Figure 9: Half power bandwidth method.

The frequencies  $f_n$ ,  $f_1$  and  $f_2$  from the frequency response function provide the damping ratio expressed in Equation (7) with the use of the half-power bandwidth method.



---

$$\xi = \frac{f_2 - f_1}{2f_n} \quad (7)$$

The Rayleigh damping coefficient can be obtained by inserting the two modes,  $\omega_1$  and  $\omega_2$  and the damping ratio ( $\xi$ ) in Equation (6).

### 3 Validation of Fluid Simulations

The chapter explores a comparison between two damping scenarios, namely translatory and rotary damping, using both analytical and simulation methods. The main focus is on the concept of the translatory damping coefficient in viscous damping and its relationship with the velocity of an object moving through a fluid. Additionally, the chapter explains the iterative approach employed to calculate the translatory damping coefficient and its utilization in determining the terminal velocity of an object. The chapter also discusses the iterated damping coefficient and the damping coefficient obtained from a Smoothed Particle Hydrodynamics analysis.

Furthermore, the chapter explores the concept of the rotary coefficient of viscous damping, which relates to the damping experienced by a rotating shaft caused by fluid resistance. A theoretical model is recreated in Abaqus to facilitate a comparison of the rotary damping coefficients.

#### 3.1 Translatory Coefficient of Viscous Damping

This subsection compares an iterated damping coefficient with a damping coefficient obtained from an SPH analysis in Abaqus. The model is made simple to be able to focus on the important aspects of the comparison. A cylindrical object is falling with the circular projected area faced in the negative  $y$ -direction. The theoretical illustration of the mobile cylinder is seen in Figure 10.

Table 1: Translatory model material data

Model Geometry and Material Properties	Value
Projected Area, mobile cylinder	$5.0 \times 10^{-5} \text{ m}^2$
Mass, mobile cylinder	0.0032 kg
Diameter, $d$	0.008 m
Diameter, $D$	0.02 m
Height, $h$	0.008 m
Fluid Density, $\rho$	$1000 \text{ kg/m}^3$
Dynamic Viscosity, $\mu$	$0.1 \text{ Ns/m}^2$
Eos, $c_0$	1500 m/s

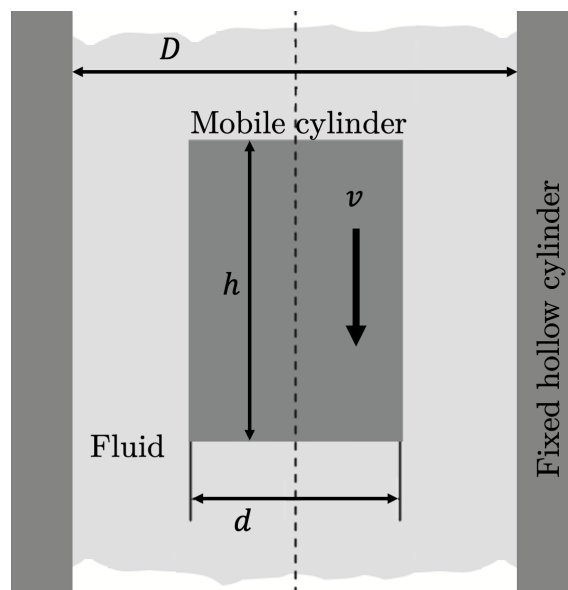


Figure 10: The mobile cylinder through a hollow cylinder filled with viscous fluid.

Source: [5]

---

## Iterated Translatory Damping Coefficient

To calculate the damping coefficient of an object through a fluid analytically, the drag force ( $F_d$ ) is required due to the equation  $c_t = -F_d/v$ . There is a circular dependency between the drag coefficient ( $C_d$ ) and the velocity ( $v$ ) of the object relative to the fluid, as both are needed to calculate the Reynolds number, which in turn is used to find translatory damping coefficient ( $c_t$ ). To break this circular dependency, an iterative approach can be used. Starting the process by making an initial guess for the velocity and then using that velocity to calculate  $Re$  and  $C_d$ , where  $C_d$  depends on  $Re$ . The fluid flow assumed in the model is a laminar flow and provides a  $Re$  within this specter  $0.1 \leq Re < 1000$ . Then using the calculated  $C_d$  for a cylinder. This is needed to compute the terminal velocity of the object, using the equations from subsection 2.1.1.

The projected area of the object is  $5.0 \times 10^{-5} \text{ m}^2$ , and the fluids density is  $1000 \text{ kg/m}^3$ , the weight of the mobile cylinder is  $0.003 \text{ kg}$  and the gravity constant working in the model. When the initial guess for the velocity is close enough compared to the calculated "new" terminal velocity, the analytical damping coefficient can be determined from Equation (8).

$$c_t = \frac{1}{2} \rho v C_d A \quad (8)$$

By following these steps, the process can be illustrated as a sheet in Excel with the given geometrical/material properties and with the formulas applied. The iterative approach is shown in Figure 11 step by step. The first terminal velocity guess resulted in a difference of  $0.34 \text{ m/s}$  compared with the "new" terminal velocity. Continuing iterating provides a translatory damping coefficient  $c_t = 0.0264 \text{ Ns/m}$  at a converging terminal velocity of  $0.85 \text{ m/s}$ . It is also interesting to compare the drag coefficient obtained in the iterative process, which results in a drag coefficient  $C_d = 1.24$  where the theoretical drag coefficient to a short cylinder shape is  $1.15$ .

Iterated Damping Coefficient					
Initial guess of velocity [m/s]	$0.1 \leq Re < 1000$	Cd	Ct [Ns/m]	New velocity [m/s]	Difference
0,250	20	2,5263	0,0159	0,594	-0,34
0,300	24	2,2481	0,0169	0,630	-0,33
0,350	28	2,0427	0,0180	0,661	-0,31
0,400	32	1,8839	0,0189	0,688	-0,29
0,450	36	1,7569	0,0199	0,712	-0,26
0,500	40	1,6526	0,0208	0,734	-0,23
0,550	44	1,5652	0,0216	0,755	-0,20
0,600	48	1,4906	0,0225	0,773	-0,17
0,650	52	1,4260	0,0233	0,791	-0,14
0,700	56	1,3695	0,0241	0,807	-0,11
0,750	60	1,3196	0,0249	0,822	-0,07
0,800	64	1,2750	0,0256	0,836	-0,04
0,850	68	1,2349	<b>0,0264</b>	0,850	0,00
0,900	72	1,1987	0,0271	0,862	0,04
0,950	76	1,1657	0,0278	0,874	0,08
1,000	80	1,1355	0,0285	0,886	0,11
1,050	84	1,1077	0,0292	0,897	0,15
1,100	88	1,0821	0,0299	0,908	0,19
1,150	92	1,0583	0,0306	0,918	0,23
1,200	96	1,0362	0,0313	0,927	0,27
1,250	100	1,0156	0,0319	0,937	0,31
1,300	104	0,9963	0,0326	0,946	0,35
1,350	108	0,9782	0,0332	0,955	0,40
1,400	112	0,9611	0,0338	0,963	0,44
1,450	116	0,9451	0,0344	0,971	0,48
1,500	120	0,9299	0,0351	0,979	0,52

Figure 11: An overview of an iterative translatory damping coefficient  $c_t$  calculation.

---

## Translatory Damping Coefficient Obtained from SPH Analysis

Now that the analytical damping coefficient is calculated, the next step is to compare it with the damping coefficient obtained from the SPH analysis and examine their correspondence.

Abaqus FEA offers various simulation possibilities, including the SPH method explained in subsection 2.2.1. To perform an SPH analysis, a similar model to the analytical one is created, including a mobile cylinder with a specified projected area. The fluid properties such as dynamic viscosity, density, and equation of state values must be specified. Once the assembly is ready, the interaction between the particles and the object using a particle set for the fluid is defined. Load conditions like gravity and appropriate boundary conditions for the analysis are specified. The solid-fluid part is determined into particles. Partition and mesh are defined using an explicit element type. Dynamic explicit analysis with a specific time step and the desired number of iterations is chosen to run the SPH analysis successfully.

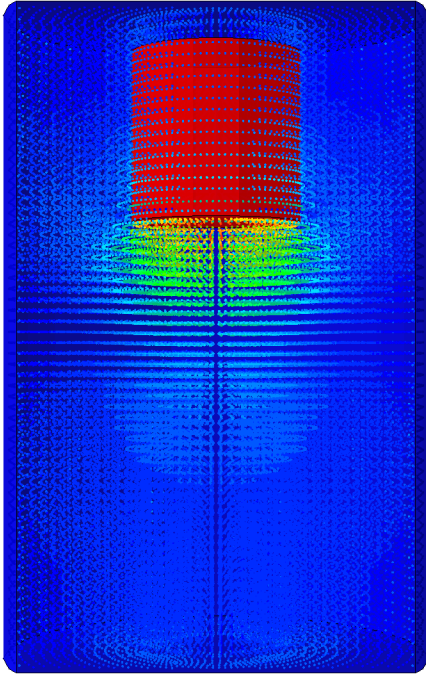


Figure 12: SPH; Start position

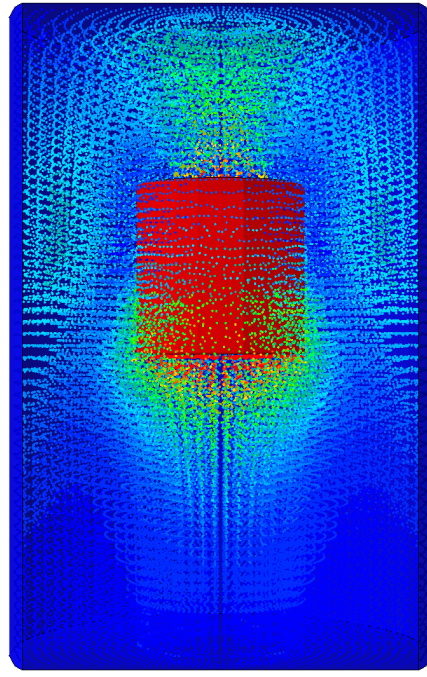


Figure 13: SPH; End position

The velocity of the mobile cylinder through the viscous fluid can be extracted from the output data of the SPH analysis, allowing a velocity-time graph where the terminal velocity can be determined. The drag coefficient and Reynolds number are calculated as previously done in the analytical method with the SPH output data. With the material properties and geometry of the mobile cylinder, Equation (8) can be used to calculate the translatory damping coefficient obtained from the SPH analysis.

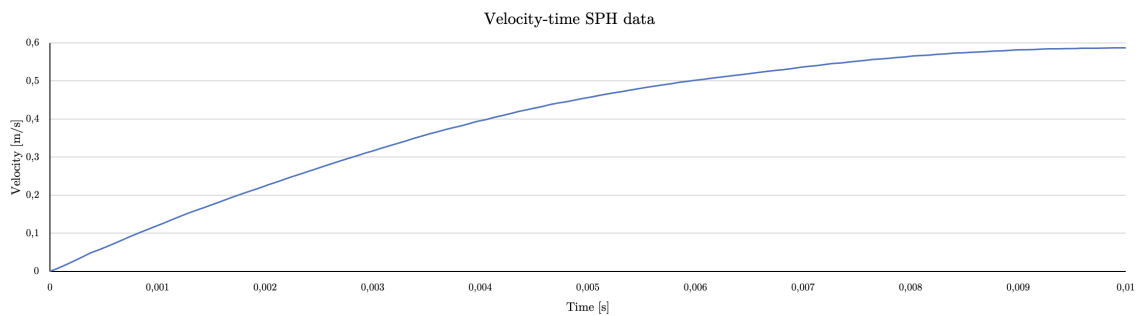


Figure 14: Velocity-time plot of the cylinder moving along the  $y$ -axis.

Figure 14 brings the terminal velocity of the cylinder to light, where it converges approximately at a velocity of 0.6 m/s. The terminal velocity from the SPH analysis is lower compared with the analytical terminal velocity, resulting in a lower translatory damping coefficient  $c_t = 0.0225$  Ns/m.

### 3.2 Rotary Coefficient of Viscous Damping

The investigation of the rotary damping coefficient is of interest, despite the fact that the rotary motion does not directly occur in the silent tool. This is due to the interaction between the shaft and the fluid. The approach involves first determining an analytical rotary damping coefficient, and then creating a model in Abaqus that uses the same material properties and geometric specifications taken from Table 2. The theoretical rotary-motion damping model is illustrated as a journal bearing in Figure 15.

Table 2: Rotary model material data

Model Geometry and Material Properties	Value
Shaft diameter, $d$	0.004 m
Bearing diameter, $D$	0.0046 m
Length, $l$	0.01 m
Fluid Density, $\rho$	1000 kg/m <sup>3</sup>
Dynamic Viscosity, $\mu$	0.1 Ns/m <sup>2</sup>
Eos, $c_0$	1500 m/s

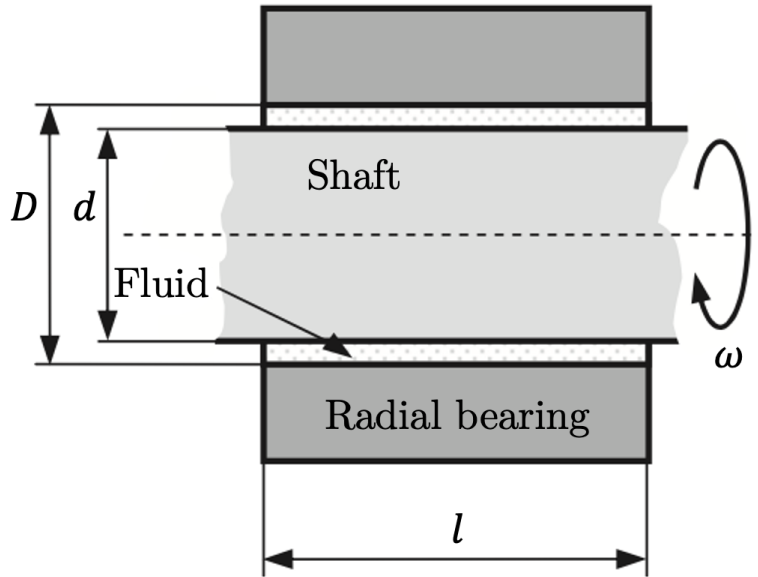


Figure 15: Rotary-motion damping for a journal bearing.

Source: [5]

#### Theoretical Rotary Damping Coefficient

The moment ( $m_d$ ) in rotary damping opposes the relative motion and is directly proportional to the corresponding relative velocity. The viscous damping moment for rotation is defined as  $m_d = c_r \omega(t)$ , with a constant damping coefficient ( $c_r$ ). The coefficient for rotation can be determined as a function of geometrical and material parameters for the rotary damper. These parameters

include the dynamic viscosity ( $\mu$ ) of the fluid, the length ( $l$ ), the inner diameter ( $D$ ) of the radial bearing, and the outer diameter ( $d$ ) of the shaft.

Since the tangential velocity of the piston's lateral surface is equal to the product of the angular velocity and the radius, the damping force resulting from the rotary motion can be expressed as shown in Equation (9).

$$f_d = c_t \omega \frac{d}{2} \quad (9)$$

Translation damping coefficient is  $c_t = \mu A/g$  where  $g$  is the gap between the two surfaces, the rotary damping force can be written as  $f_d = \pi \mu d^2 l \omega / D - d$ . The resulting damping torque is provided in Equation (10).

$$m_d = \frac{\pi \mu d^3 l}{2(D-d)} \omega \quad (10)$$

When comparing damping moment  $m_d = c_r \omega(t)$  and the damping torque equation, the resulting rotary damping coefficient is expressed in Equation (11).

$$c_r = \frac{\pi \mu d^3 l}{2(D-d)} \quad (11)$$

The resulting theoretical coefficient for rotational damping is calculated  $c_r = 1.68 \times 10^{-8}$  Nms with given properties/dimensions from the Table 2.

### Rotary Damping Coefficient Obtained from SPH Analysis

Figure 16 illustrates an assembly consisting of three parts: the bearing, the shaft, and the fluid. The fluid is assigned material properties similar to those used in the analytical approach. To examine the rotary damping coefficient, a torque for rotation is employed. To apply torque to the shaft, a coupling with a defined reference point is created. After applying the interaction type and mesh, a dynamic explicit step with a varying time period is simulated. The duration of the time period varies due to the changing torque, requiring both shorter and longer dynamic analyses to obtain the terminal rotary velocity. Applying a torque ranging from 0.01 Nm up to 1.0 Nm in the  $CM1$ -direction (shown in Figure 15), to run several analyses.

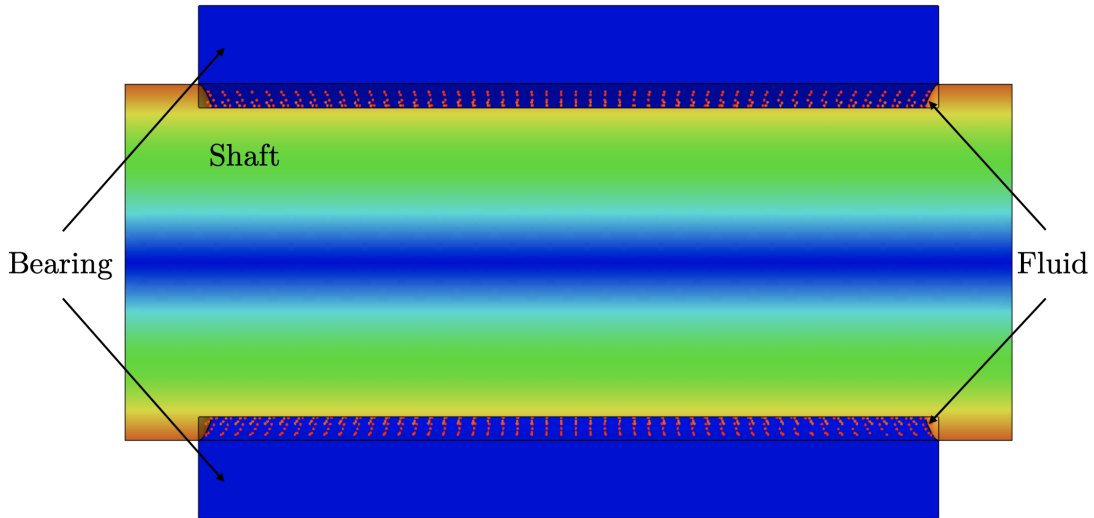


Figure 16: View cut of the rotary model in Abaqus.

In Abaqus, the torque ( $m_d$ ) is defined as a load prior to conducting the SPH analysis. The resulting output data allows for the plotting of the rotary motion of the shaft. To visualize the rotary motion, a node-set is created at the outer edge of the shaft. By plotting the amplitude of this specific node over the given time period, the rotary motion of the shaft becomes apparent. Figure 17 depicts one of the simulations where the effect of increased torque on the frequency, with two different torque values, is illustrated. It is evident that higher torque results in a more rapid frequency.

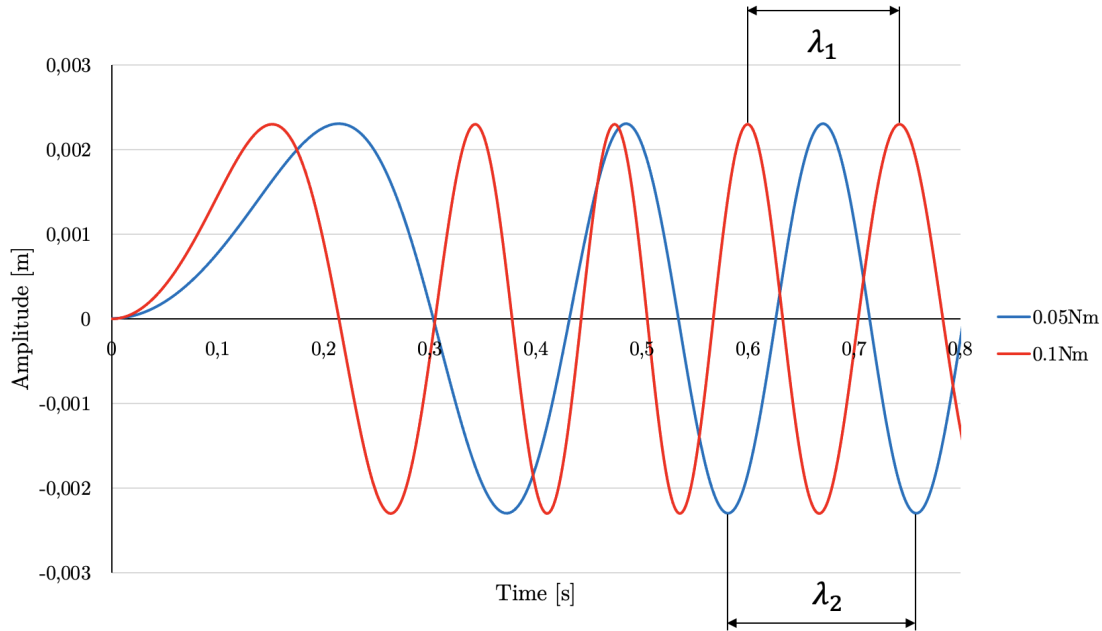


Figure 17: Rotary motion of the shaft with two different torques applied. Red; 0.10 Nm. Blue; 0.05 Nm.

When a torque of 0.1 Nm is applied, it results in a rotational frequency ( $n$ ) of 7.1 cycles/second due to a wavelength of  $\lambda_1 = 0.14$  s. This, in turn, yields a tangential velocity of  $v = 0.10$  m/s. The tangential velocity is determined by multiplying the angular velocity by the radius, with the radius assumed to be the distance between the parallel surfaces. The angular velocity ( $\omega$ ) is calculated by dividing the angular displacement ( $\theta$ ) by the time. These calculations are detailed in Appendix A.

In contrast, when a torque of 0.05 Nm was applied, a longer wavelength of  $\lambda_2 = 0.18$  s was observed, resulting in both a lower rotational frequency 5.6 cycles/second and tangential velocity of  $v = 0.08$  m/s. This process was repeated eight times for different applied torque values, and a plot was generated to illustrate the relationship between applied torque and tangential velocity. Notably, the rotary damping coefficient for each applied torque showed an increasing trend.

Figure 18 demonstrates a correlation between tangential velocity and torque, indicating that the velocity increases with higher torque values. The curve exhibits a steep incline at lower torque values, followed by a gradual plateau as torque increases further. It is important to note that the rotary damping coefficient did not exhibit linear growth. For instance, at an applied torque of 0.01 Nm, the rotary damping coefficient was  $6.8 \times 10^{-4}$  Nms/rad, which increased to  $7.2 \times 10^{-3}$  Nms/rad when the torque was 1.0 Nm.

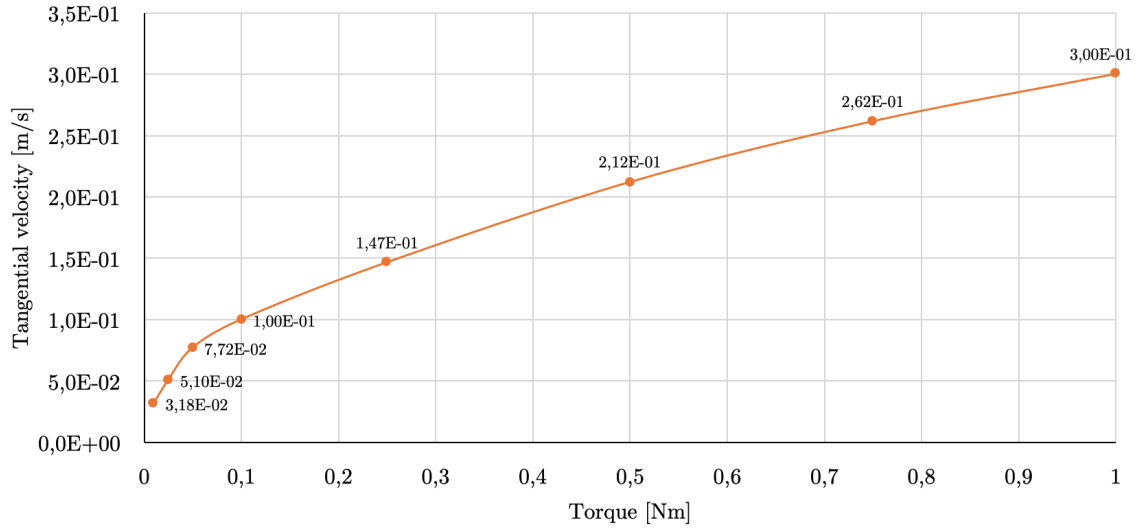


Figure 18: Correlation between tangential velocity and torque.

### 3.3 Fluid Simulations Summary

The translatory damping coefficient ( $c_t$ ) yielded approximately similar values through both analytical and SPH simulation methods. The analytical approach, employing an iterative method, determined a translatory damping coefficient of 0.0264 Ns/m, while the SPH simulations resulted in a coefficient of 0.0225 Ns/m.

However, the comparison of rotary damping coefficients ( $c_r$ ) did not align. The analytical calculations produced a rotary damping coefficient of  $1.68 \times 10^{-8}$  Nms. On the other hand, when a model was recreated in Abaqus, maintaining similar dimensions and fluid properties, the resulting rotary damping coefficient varied from  $6.8 \times 10^{-4}$  Nms/rad to  $7.2 \times 10^{-3}$  Nms/rad due to different applied torques. Consequently, the simulated coefficient exhibited larger values compared to the analytical coefficient, showcasing the impact of varying coefficients.



---

## 4 Spring/Dashpot in Abaqus

There are multiple methods to experiment with the spring/dashpot feature. Since the accessible Abaqus package does not allow frequency response analysis while using the SPH method, the chapter explores the verification of the dashpot feature in Abaqus as an alternative approach. One of the elaborated methods is to run several frequency response analyses of a 2DOF model with varying dampening input parameters. The model used in this section is a massive steel bar that is fixed at one end with an added mass at the other end. The mass is not physically connected to the bar, it is connected by a two-point spring/dashpot element. The output data from the FRF analyses is used to observe the change in magnitude and natural frequency with the change in spring/dashpot input.

### 4.1 Experimental Spring/Dashpot Testing

To be comfortable using the spring/dashpot element in Abaqus, it is essential to work gradually towards the confident use of this feature. By for example focusing on the spring element as the first step, it allows the possibility to observe how a simple 2DOF model (Figure 19) will react while varying the stiffness in the spring element.

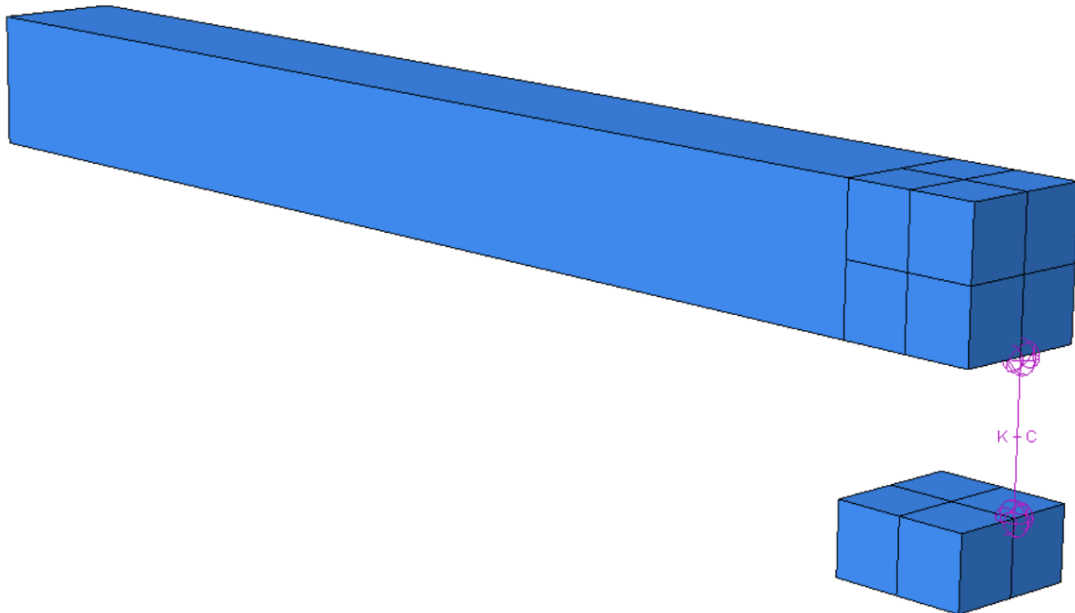


Figure 19: Theoretical 2DOF square bar model with attached mass

Modeling a square bar ten times the height/width with a box attached under the tip makes it possible to recreate a model representing the theoretical 2DOF model. The defined material for this model is steel with Young's modulus of  $210 \times 10^9 \text{ N/m}^2$  and a Poisson's ratio equal 0.28. The defined density of steel is  $8050 \text{ kg/m}^3$ . The box is the dampening mass ( $m_2$ ) which is connected to the square bar with a spring/dashpot element, representing the stiffness ( $k_2$ ) and damping coefficient ( $c_2$ ). The mass is restricted to only being allowed to move along the tool's direction of motion, which is in the  $y$ -direction. The spring/dashpot element is positioned at the tool's end, where the equivalent modal mass is computed. It represents the cutting force in the model, aiming to establish similarity with the theoretical model and verify if the Frequency Response Functions match between the two.

Figure 20 illustrates an exponential growth of the magnitude peaks when increasing the stiffness

( $k_2$ ) in the spring element. Also interesting is the natural frequency increasing corresponding with an increased stiffness from  $1.5 \times 10^5$  N/m to  $5.0 \times 10^5$  N/m. It is clearly the system is not optimized against large magnitude peaks.

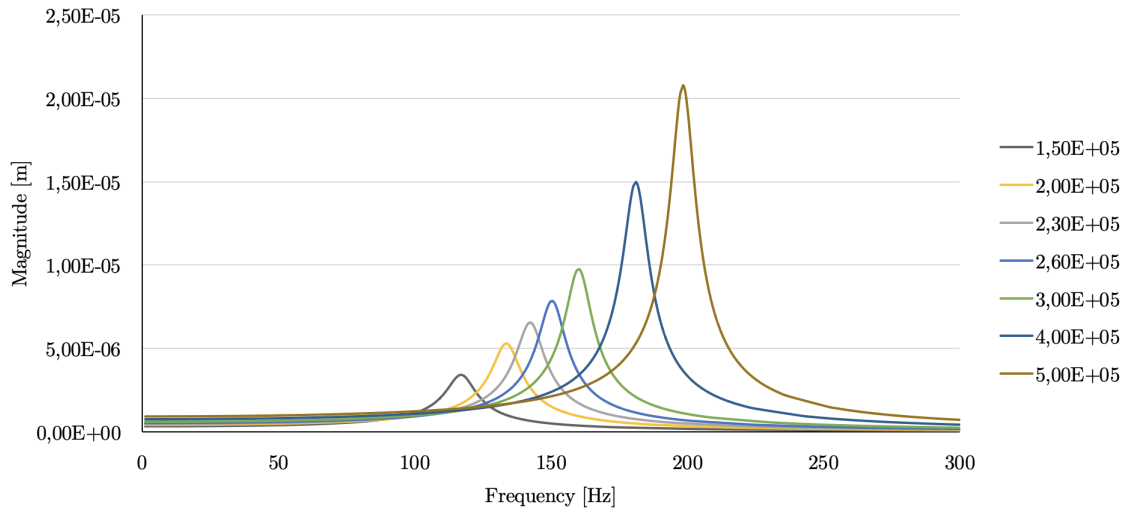


Figure 20: Experimenting the effect of changing the stiffness in the spring element

By inserting a dashpot value, the FRF changes as shown in Figure 21. By increasing the spring element while obtaining the same dashpot element, it can be seen that in the three curves with  $c_2 = 20$  Ns/m, the peaks begin to equalize each other while increasing the stiffness. Brown curve ( $k_2 = 3.20 \times 10^5$  N/m,  $c_2 = 20$  Ns/m) shows an FRF with two approximately equal heights but is not optimized due to the complexity of an optimized two-mass system. Alternatively, if the dashpot element is set to a high value, the curves with  $c_2 = 140$  Ns/m show higher amplitudes on the left peak compared to the right peak. This occurs because there is too much damping applied to the system.

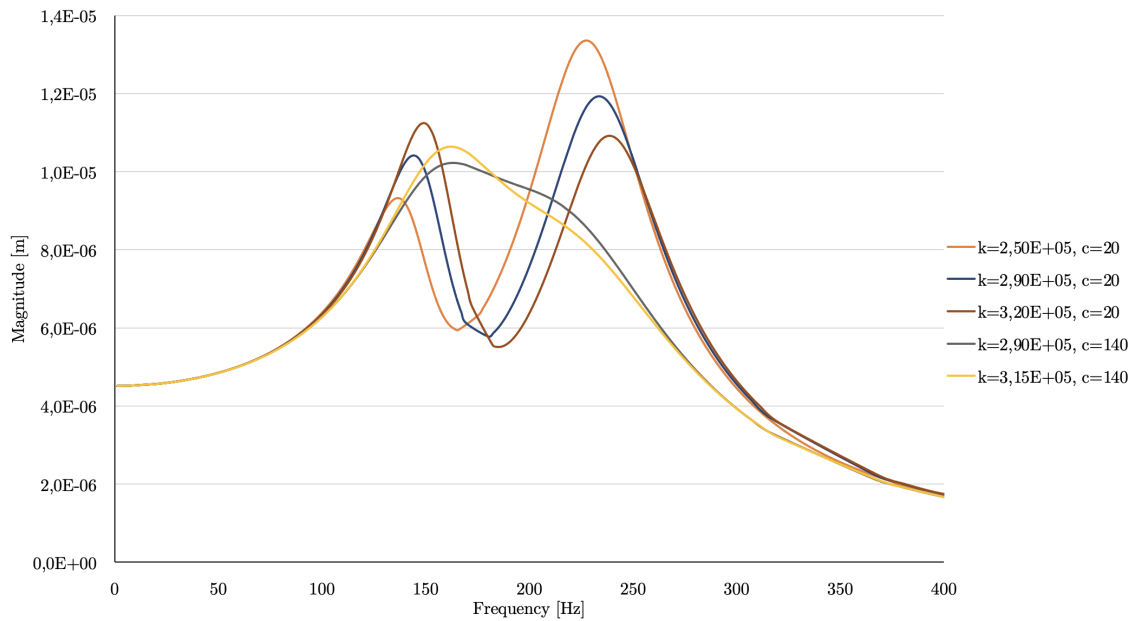


Figure 21: Experimenting with the effect of changing spring/dashpot parameters.

To connect this founding with a theoretical 2DOF FRF calculated in Matlab, some parameters of the square bar are needed. To find the  $k_1$ -value in Abaqus is to run static deflection analysis of the square bar alone illustrated in Figure 22. The bar is fixed at one end and applied with a force  $F = 10\text{ N}$  at a defined coupling constraint at the tip of the tool working in negative  $y$ -direction. Resulting in a maximum deflection  $x = 4.86 \times 10^{-6}\text{ m}$ . It provide the tool stiffness,  $k_1 = 2.06 \times 10^6\text{ N/m}$  when using Hooke's law  $k_1 = F/x$ .

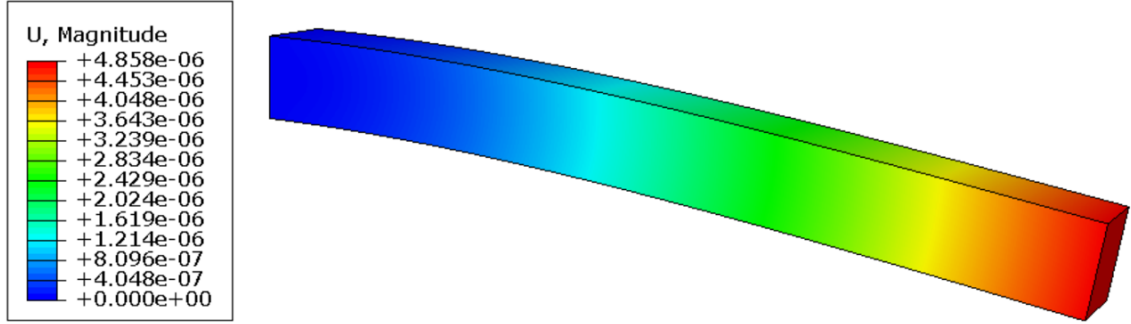


Figure 22: Static deflection analysis with an applied load at the tip

To calculate the equivalent modal mass ( $m_1$ ), the natural frequency of the 1DOF model must be determined through a frequency simulation. Resulting in four modes shown in Figure 23 whereas the first two modes have the same frequency value due to symmetry in the structure. Mode 3 and 4 are not taken into consideration due to their natural frequencies outside the project's frequency range. The natural frequency ( $f_n$ ) of the square bar is, therefore, 203.9 Hz. The equivalent modal mass  $m_1 = k_1/\omega_n^2$ , where  $\omega_n$  is  $f_n 2\pi$ , is then equal to 1.25 kg.

Frame	
Index	Description
0	Increment 0: Base State
1	Mode 1: Value = 1.64074E+06 Freq = 203.86 (cycles/time)
2	Mode 2: Value = 1.64074E+06 Freq = 203.86 (cycles/time)
3	Mode 3: Value = 5.91064E+07 Freq = 1223.6 (cycles/time)
4	Mode 4: Value = 5.91064E+07 Freq = 1223.6 (cycles/time)

Figure 23: Eigenvalues obtained from frequency analysis in Abaqus

To calculate the damping coefficient ( $c_1$ ), the tool stiffness ( $k_1$ ), equivalent modal mass ( $m_1$ ), and a damping ratio ( $\xi$ ) are required. By using the half-power bandwidth method, the damping ratio can be determined by using Equation (7) with the data represented in Figure 24. The damping coefficient  $c_1 = 2\xi\sqrt{k_1 m_1}$  is calculated equal to 64.8 Ns/m.

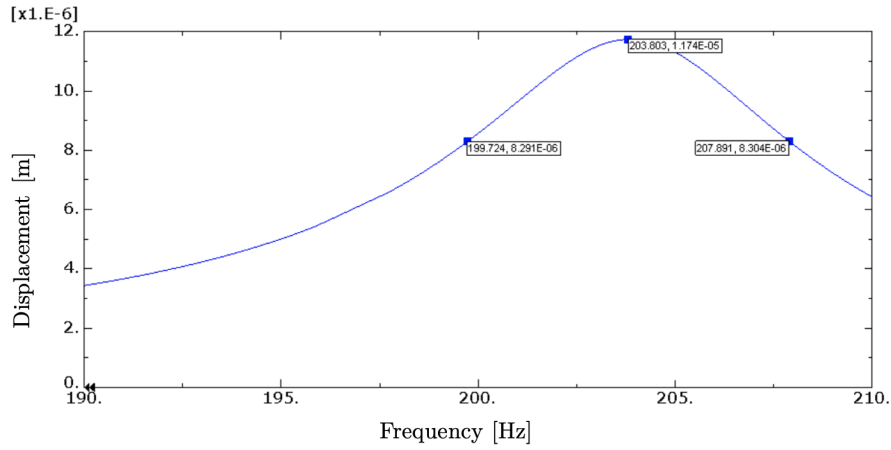


Figure 24: FRF of the bar to find Rayleigh damping coefficients

With the damping ratio and eigenvalues calculated for this model, it provides the Rayleigh damping coefficients as following  $\alpha = 0.04$  and  $\beta = 0.000028$  by using Equation (6) illustrated in Figure 25.

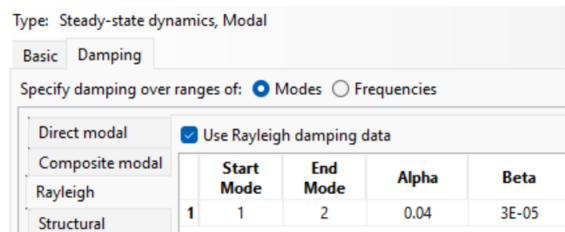


Figure 25: Rayleigh coefficient defined in the modal steady-state step.

With the calculated equivalent modal mass, tool stiffness, and the damping coefficient, the optimized stiffness ( $k_2$ ) and damper ( $c_2$ ) can be obtained in Matlab with a dampening mass ( $m_2$ ) equal 0.25 kg. It provides an optimized  $k_2$ -value ( $2.89 \times 10^5$  N/m) and  $c_2$ -value (141 Ns/m). The resulting FRF from Matlab is illustrated in Figure 27 (a). Now with the optimization obtained from Matlab, they are inserted in the spring/dashpot element seen in Figure 26.

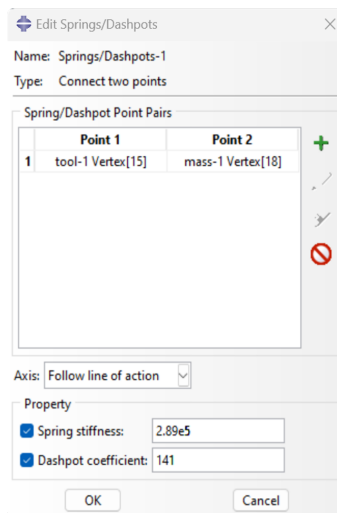


Figure 26: Spring/Dashpot point pairs between tool and mass with given input parameters.

After incorporating the necessary components such as material properties, sections, mesh, and load conditions, the analysis begins with a frequency analysis. Subsequently, a dynamic steady-state analysis is conducted to obtain the FRF from the simplified 2DOF model. This approach allows for a comprehensive assessment of the system's response under dynamic conditions. The resulting FRF of the model with the defined spring/dashpot element is illustrated in Figure 27 (b).

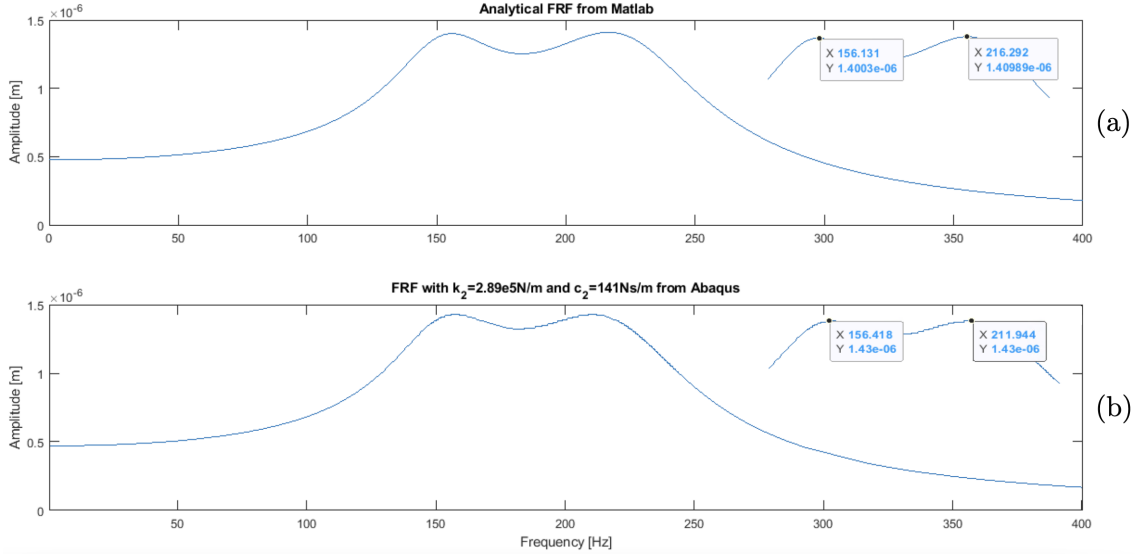


Figure 27: Frequency response function. (a); Analytical Matlab plot. (b); Spring/dashpot plot from Abaqus.

It is interesting to observe how the spring/dashpot feature aligns with the analytical results. Both plots show an optimized FRF with two peaks at similar frequencies. The right peak differs by only 0.3 Hz, while the left peak has a difference of 4.4 Hz. Additionally, the amplitude results between the Matlab plots and the spring/dashpot are consistent, with both showing an amplitude of  $1.4 \times 10^{-6}$  m.

## 4.2 Verify Dashpot Element

It is interesting to compare the dashpot element without the spring taken into consideration with an analytical approach compared to a frequency response analysis in Abaqus. This is to be comfortable using the dashpot element for later combining multiple findings as elaborated in section 6.

Comparing the dashpot element, specifically without considering the spring component, using both an analytical approach and frequency response analyses in Abaqus yields interesting insights. This comparison helps enhance the understanding of the dashpot element's behavior and enables the possibility of combined results into more complex models, as discussed in section 6.

The method used is by calculating the viscous damping coefficient ( $c$ ) from a single degree of freedom model to verify the dashpot element in Abaqus. Comparing the analytical viscous damping coefficient using the velocity and acceleration output from a dynamic explicit analysis with the dashpot element input in Abaqus.

An example of an analytical method to derive the viscous damping coefficient can be calculated with a damped lumped parameter model as shown in Figure 28. The equation obtained from the free body diagram is written in Equation (12).

$$m\ddot{x} + c\dot{x} = f \quad (12)$$

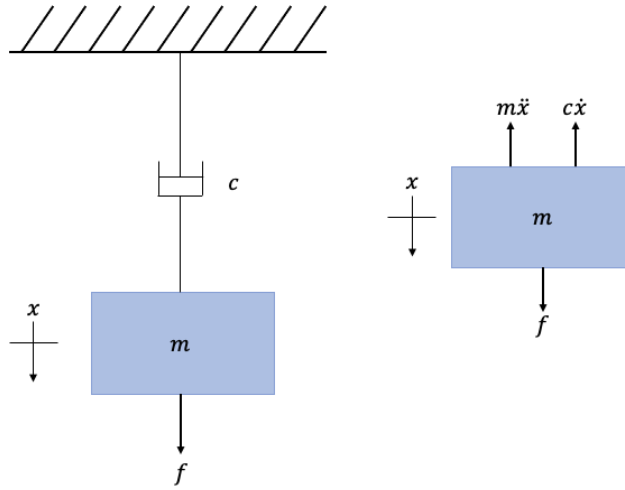


Figure 28: Single degree of freedom. Left; Damped lumped parameter model. Right; Free body diagram.

From Equation (12) the viscous damping coefficient can be expressed as shown in Equation (13).

$$c = \frac{f - m\ddot{x}}{\dot{x}} \quad (13)$$

To compare the theoretical damping coefficient with the dashpot element in Abaqus, the order of approach is dependent on each other. The theoretical damping coefficient depends on the velocity and acceleration of the mass from Abaqus. The output data providing this is a result of dynamic explicit analysis with an already applied damping coefficient in the dashpot element. The Abaqus model (Figure 29) is created similarly to the damped parameter model, with a defined load in the negative  $y$ -direction. The defined dashpot element is applied between the rigid body and the mass with a damping coefficient equal 0.10 Ns/m. Given the material properties from the analytical calculation, the weight of the mass in the Abaqus model is similar. The field output from the dynamic explicit analysis provides a time-dependent velocity/acceleration graph of the moving mass.

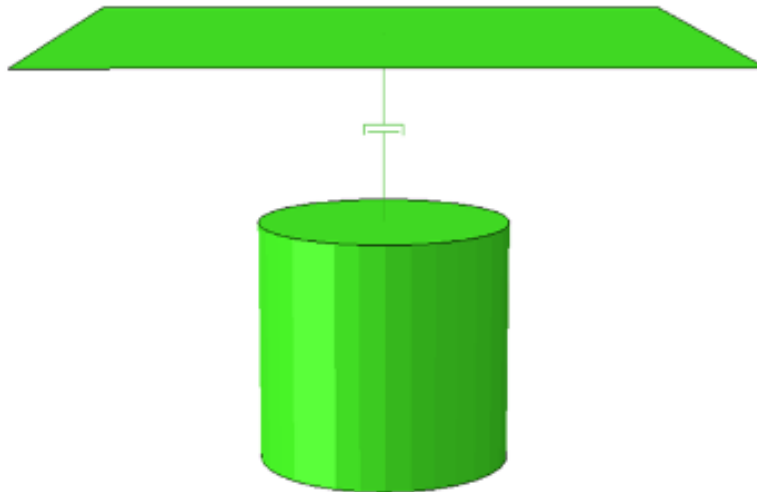


Figure 29: Single degree of freedom model, dashpot element illustrated.

To find the acceleration ( $\ddot{x}$ ), one can divide the difference in initial and final velocity by the time period. Resulting in an acceleration equal 7.8 m/s<sup>2</sup> and the average velocity ( $\dot{x}$ ) is 0.06 m/s.

---

The applied load ( $f$ ) is 0.032 N and the weight of the mass ( $m$ ) is 0.00324 kg. This allows for a comparison between the analytical viscous damping coefficient and the defined dashpot element used in Abaqus. The viscous damping coefficient can be calculated using Equation (13) resulting in an analytical damping coefficient equal 0.11 Ns/m.

### 4.3 Spring/Dashpot Summary

The validation process of the spring/dashpot element yielded promising outcomes. Initially, various input parameters were experimented to observe their effects on the FRF. Subsequently, the model in Abaqus was compared with a theoretical two-mass system in Matlab. The correspondence between the two graphs was encouraging, confirming that the spring/dashpot element behaves as expected in Abaqus. Specifically, the FRF exhibited two peaks with equal amplitude in the same frequency range.

In terms of validating the dashpot element independently, the resulting damping coefficient was found to be similar to the theoretical damping coefficient in a one-mass system. This indicates that the dashpot element accurately reflects the expected damping behavior in the specific scenario compared.

---

## 5 Rubber Testing and Simulating

This section focuses on simulating the damping effect in rubber materials through an impact simulation. The objective is to investigate the influence of Rayleigh coefficients on the damping properties of rubber. In the first subsection, the damping primarily occurs due to the vertical movement of the rubber, without experiencing any shear loads. This allows a specific focus on the damping coefficients. In the following subsection, a shear load is applied to rubber elements to examine the comparison between the shear stiffness by varying Young's modulus for both models with one and two rubber elements.

### 5.1 Damping Consideration and Impact Simulation

This subsection presents a detailed procedure for determining the Rayleigh damping coefficients of a structure. To obtain these coefficients, a simplified model is constructed, comprising a rubber element with a mass attached, as depicted in Figure 30. An implicit dynamic analysis is performed to simulate an impact scenario involving the model. By applying an external force to the model, the rubber element acts as an energy absorber. The objective is to examine how the Rayleigh coefficients influence the time-domain attenuation curve in comparison to the model without defined Rayleigh coefficients. Prior to initiating the impact analysis, a frequency analysis and an FRF analysis are conducted to determine the eigenvalues and damping ratio.

Using Equation (7) where the natural frequency and maximum and minimum frequency corresponding to the  $A_{max}/\sqrt{2}$  is inserted to estimate the damping ratio. This is obtained from a steady-state dynamic analysis as elaborated in subsection 2.5. After a frequency response analysis of the rubber model, frequency data is obtained and resulting in a damping ratio  $\xi = 0.058$ . With the damping ratio calculated, the Rayleigh coefficients  $\alpha$  and  $\beta$  can be estimated by using Equation (6) with the given mode frequencies  $\omega_1 = 112.7\text{ Hz}$  and  $\omega_2 = 372.2\text{ Hz}$ . As the damping ratio is dimensionless, a consistent unit is employed for all frequencies used in the calculations of Rayleigh coefficients, such as hertz in this case. The mode frequencies are obtained through a frequency analysis in Abaqus, resulting in the determination of two eigenvalues, as depicted in Figure 30.

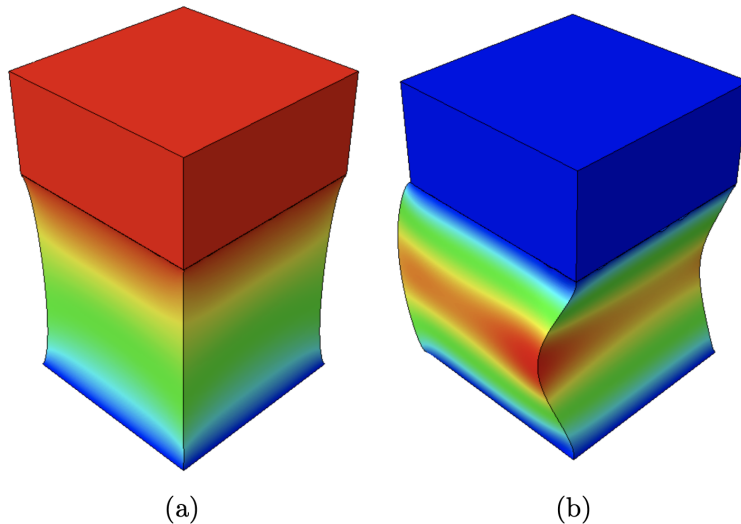


Figure 30: The two frequency modes response along  $y$ -direction. (a); First mode shape ( $\omega_1 = 112.2\text{ Hz}$ ). (b); Second mode shape ( $\omega_2 = 372.2\text{ Hz}$ ).

The resulting Rayleigh coefficients are calculated in Equation (14) and provide  $\alpha = 10.05$  and  $\beta = 0.00024$ .



$$\begin{Bmatrix} \alpha \\ \beta \end{Bmatrix} = \frac{2 \cdot 0.058}{112.2 \text{ Hz} + 372.2 \text{ Hz}} \begin{Bmatrix} 112.2 \text{ Hz} + 372.2 \text{ Hz} \\ 1 \end{Bmatrix} \quad (14)$$

With the calculated Rayleigh coefficient, all the requested material properties are now ready to be implemented in Abaqus. The density, Poisson's ratio, and Young's modulus are filled in with the damping defined as illustrated in Figure 31.

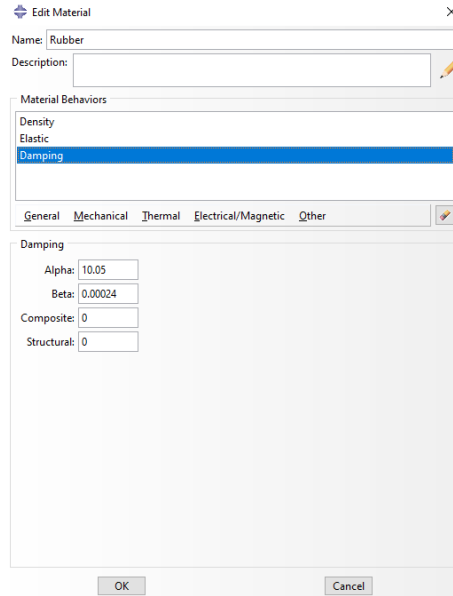


Figure 31: Rayleigh damping coefficients input for the rubber material

A dynamic implicit step is created to perform an impact simulation of the rubber model. The material properties and boundary conditions were defined. There were different methods to set up the vibration simulation, such as using an impact hammer to measure the external force and applying the same impact force in the dynamic explicit analysis. However, in this simulation, the chosen method is to pull the model a given deflection in the positive  $y$ -direction and then release it. This required two steps to simulate the motion, one static step that propagates further to the dynamic step.

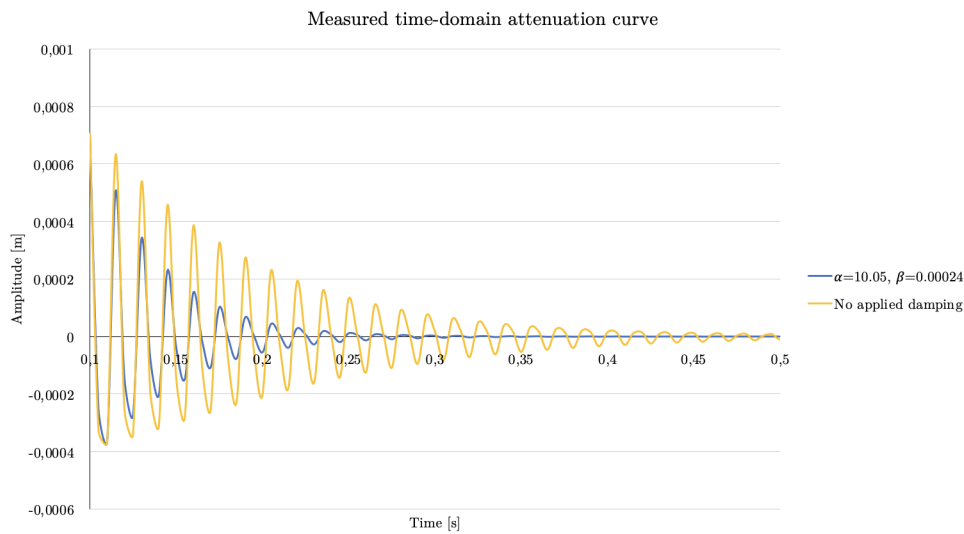


Figure 32: Amplitude deflection graphs caused by external force with and without Rayleigh damping coefficients.

The impact histories from the rubber model with and without damping applied are shown in Figure 32. The blue line in the figure shows the Rayleigh coefficient's damping effect on the rubber material. If the damping is excluded as a material property, the yellow line exhibits less damping, leading to increased amplitude deflections compared to the damped blue line.

## 5.2 Rubber Element Shear Stiffness

This section discusses the comparison of shear stiffness between one and two rubber elements. The aim is to ensure that the shear stiffness obtained in Abaqus corresponds to the stiffness obtained in Matlab. To achieve this, the stiffness needs to be calculated and verified through static analysis. The actual damper consists of a high-density mass held by two rubber elements, so the optimization code in Matlab should provide a value for  $k_2$  that represents the overall stiffness of both rubber elements in the Abaqus model. The deflection of the rubber elements is influenced by Young's modulus, which directly affects the resulting shear stiffness.

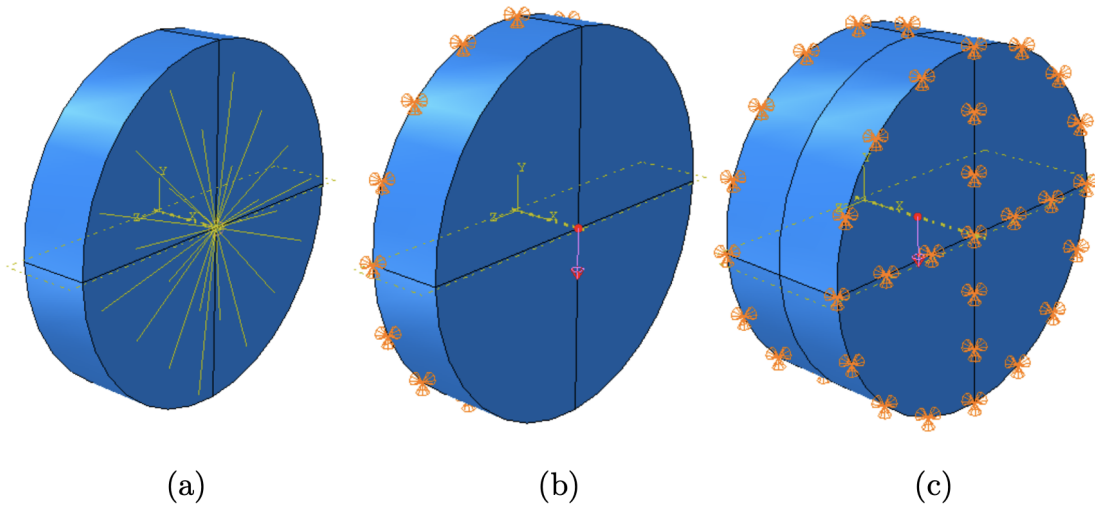


Figure 33: (a); Coupling constraint. (b); Boundary conditions for the single rubber element. (c); Boundary conditions for the model with two rubber elements.

To determine the shear stiffness of the two models, Hooke's law ( $k = F/x$ ) is utilized. The applied perpendicular load ( $F$ ) divided by the resulting deflection ( $x$ ) in the  $y$ -direction provides the shear stiffness. Both models are configured identically, with the same global size, element shape, and element family. A coupling constraint is applied to the control point representing the surface, ensuring a realistic load situation for the rubber elements, as depicted in Figure 33 (a). Regarding the boundary conditions, the load is consistent for both models, while Figure 33 (b) illustrates a single fixed surface, and Figure 33 (c) shows two fixed surfaces. The inner surfaces are connected by a tie coupling to connect the two rubber elements together.

A general static step is created with default incrementation settings to simulate the deflection. Figure 34 illustrates the deflection of both models before and after the load is applied. The primary difference in deformation between the two models occurs where the deflection takes place, owing to variations in geometry.

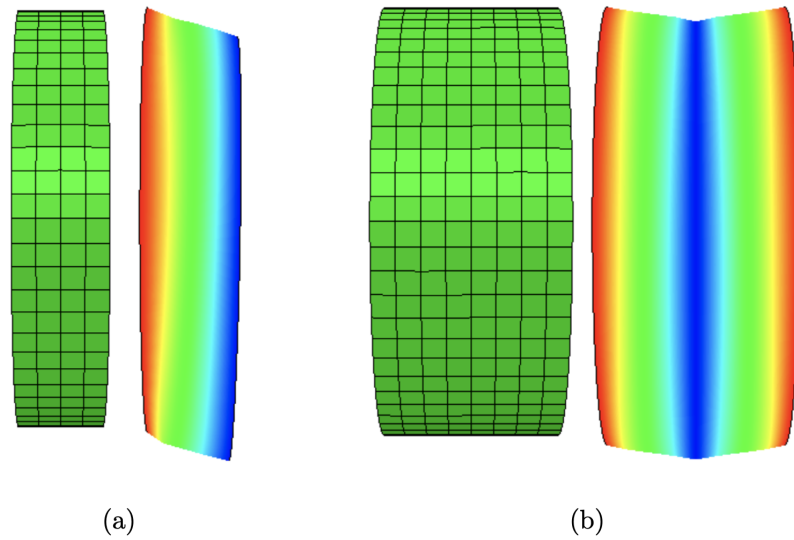


Figure 34: (a); Single rubber element before and after deformation. (b); Two merged rubber elements before and after deformation.

The purpose of this investigation is to compare the shear stiffness of both models. Theoretically, the model with two rubber elements should have a stiffness twice as large as the model with one rubber element. By increasing Young's modulus of the rubber material while keeping a constant load applied, the maximum deflection is observed to decrease linearly. Consequently, this leads to an increased shear stiffness for both models, as depicted in Figure 35.

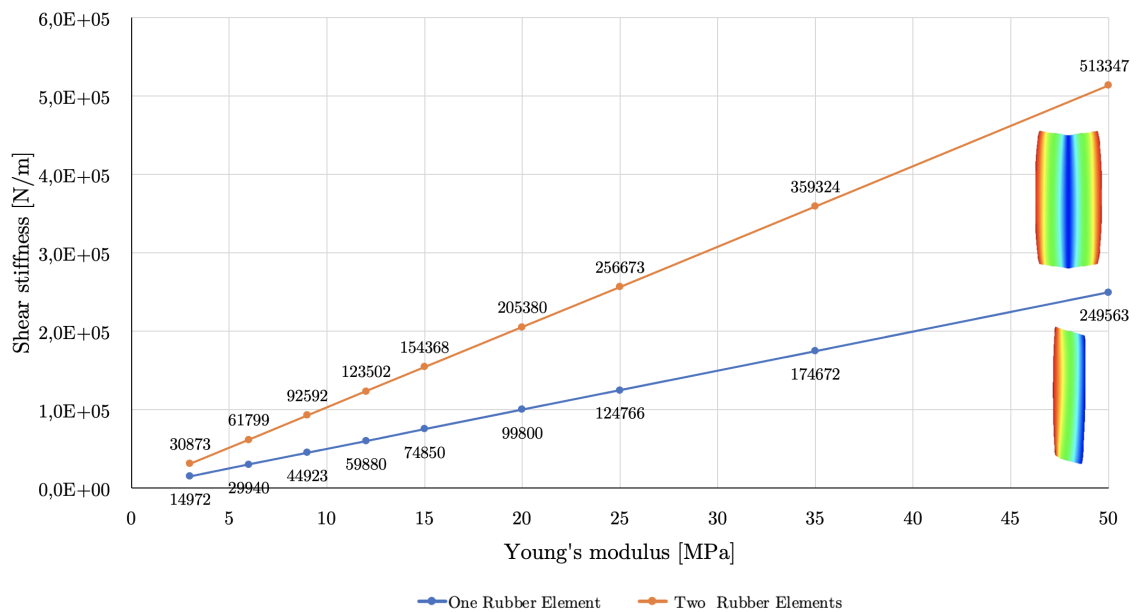


Figure 35: Blue curve; Representing model with one rubber element. Orange curve; Representing the model with two rubber elements.

The model featuring two rubber elements exhibits a shear stiffness approximately twice as large as that of the single rubber element model. The percent deviation between twice the stiffness of the single rubber element model and the shear stiffness of the two rubber element model remains approximately around 3.0%. The analysis is conducted by incrementally increasing the applied Young's modulus from  $E = 3.0 \times 10^6 \text{ N/m}^2$  to  $E = 50.0 \times 10^6 \text{ N/m}^2$ , with a total of nine intervals

---

considered for both models.

### 5.3 Rubber Element Summary

The damping effect of the rubber is confirmed by assigning Rayleigh coefficients to the material. An impact analysis was conducted on two similar setups, one with Rayleigh coefficients and the other without, and a comparison was made. The presence of these coefficients resulted in a more rapid decrease in motion within the model. These coefficients reflect the rubber's ability to absorb kinetic energy when subjected to an external force, considering the defined damping properties.

Furthermore, the rubber element exhibits a linear correlation between the shear stiffness of the model and the defined Young's modulus of the rubber. This relationship was confirmed through multiple static analyses, indicating that an increase in Young's modulus leads to an increase in shear stiffness. This approach is employed to determine the optimized stiffness  $k_2$  for the rubber elements in a two-mass system. The subsequent section will utilize this shear stiffness approach to construct a model that allows for the most accurate comparison with an analytical FRF.

---

## 6 Combined Simulations

This section presents the combined results of an FRF comparison between an analytically optimized two-mass system simulated in Matlab and a two-mass system modeled in Abaqus. The comparison focuses on the influence of the shear modulus of the rubber elements on the frequency response function. The results revealed that the theoretical model and the Abaqus model achieved an optimized FRF curve by increasing the stiffness value in Abaqus.

Furthermore, this section explores the effect of fluid on the motion of a moving mass subjected to a periodic force. The model primarily focuses on the tip of the tool, which is no longer treated as a two-mass system. In this model, the tool body remains fixed while a periodic force is applied to the moving mass, which is supported by two rubber elements immersed in the fluid. To assess whether the fluid can be realistically treated as a damping viscous fluid, the motion of the moving mass is compared with a similar model where the fluid is replaced by a dashpot element. By examining the damping coefficients the investigation determines whether the presence of either the fluid or the dashpot element provides any damping effect on the motion of the moving mass.

Table 3 presented below provides a summary of the material properties of the models discussed in this section. Regarding the meshing technique employed, Appendix B provides a detailed overview of each component.

Table 3: Material properties for steel, rubber, and fluid

Material Properties	Value
Young's modulus, steel, $E$	$210 \times 10^9, \text{N/m}^2$
Density, steel, $\rho$	$8050, \text{kg/m}^3$
Assumed damping ratio, tool body $\xi$	0.02
Poisson's ratio, steel, $\nu$	0.28
Density, rubber, $\rho$	$1060, \text{kg/m}^3$
Poisson's ratio, rubber, $\nu$	0.45
Density, fluid, $\rho$	$1000, \text{kg/m}^3$
Dynamic Viscosity, $\mu$	$0.1, \text{Ns/m}^2$
Reference sound speed, $c_0$	$1500, \text{m/s}$

### 6.1 Tuned Mass Damper Simulation

This subsection is an FRF comparison between a simplified Silent Tool and an analytical approach. The silent tool is a complex component that incorporates various features, such as the insert and channels for cutting fluid. The model used for analysis makes certain assumptions and simplifications regarding material properties and geometries. These simplifications are necessary to align the model as closely as possible with the analytical 2DOF model implemented in Matlab. The simplified silent tool is illustrated in Figure 36.

Assuming the tool body to be a massive cylinder simplifies the analysis of its equivalent modal mass ( $m_1$ ), stiffness ( $k_1$ ), and damping coefficient ( $c_1$ ). Due to its simplified geometry, calculating these parameters becomes relatively straightforward. For a massive cylinder with a length ten times its diameter, the natural frequency is determined to be 178.7 Hz. Additionally, the tool body stiffness is calculated as  $1.24 \times 10^6 \text{ N/m}$ . The equivalent modal mass can be obtained by utilizing these two parameters through the equation  $m_1 = k_1/\omega^2$ , resulting in a value of 0.98 kg. The damping coefficient is equal 44.2 Ns/m with an assumed structural damping ratio  $\xi = 0.02$ . Adjusting the material density specified for the dampening mass ( $m_2$ ) allows for modification, in this analysis  $m_2 = 0.08 \text{ kg}$ . These parameters play a crucial role in optimizing the frequency response function to achieve the most favorable outcome.

The optimization process implemented in Matlab (see Appendix C) yields optimized values for the

stiffness ( $k_2$ ) and damping coefficient ( $c_2$ ). By inserting these values, it results in an optimized stiffness value  $k_2 = 85.2 \times 10^3 \text{ N/m}$  and dampening coefficient  $c_2 = 28 \text{ Ns/m}$ .

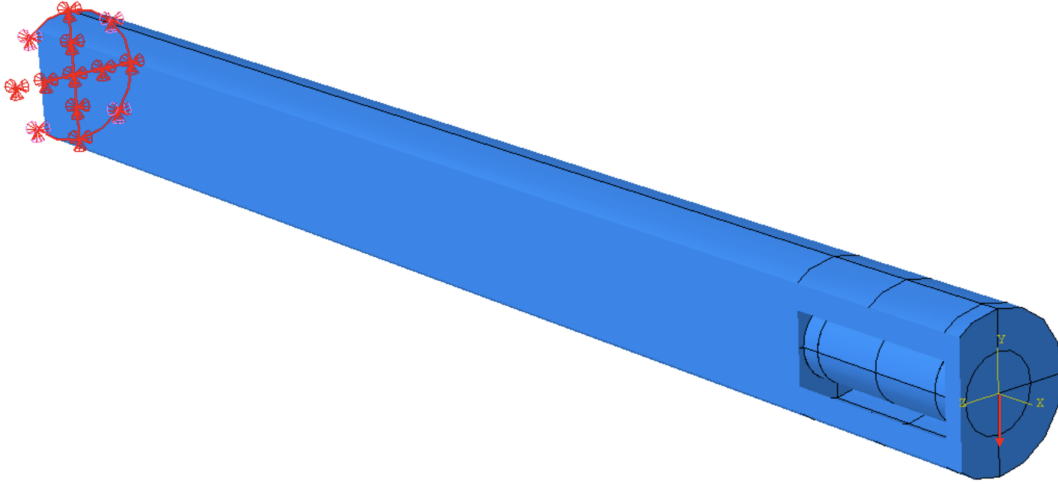


Figure 36: Boundary conditions of tool integrated with damper at the tip.

A damping mass integrated inside the tip of the tool withholds by two rubber elements and a dashpot element illustrated in Figure 37. The assembly comprises the main tool body, followed by the damping system consisting of two rubber elements and a mass. All components are connected using the "tie interaction method". The dashpot element connects the damping mass, to the tool body. In the steady-state analysis, the boundary conditions involve a concentrated force of 1.0 N applied at the tip, while the opposite end is fixed in all directions.

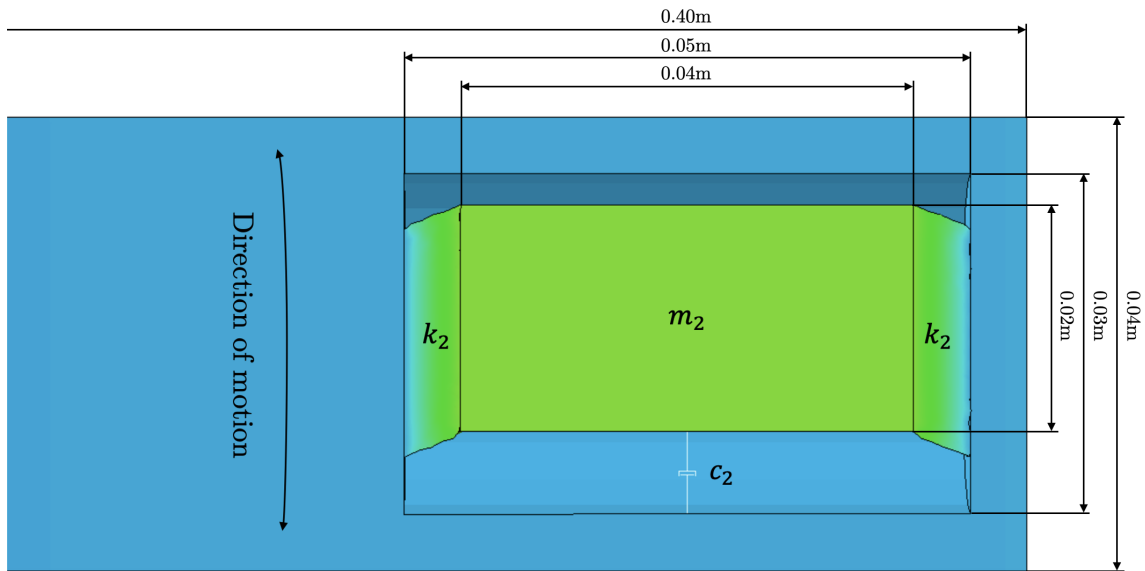


Figure 37: Cross-section of the tool's geometry.

The interesting thing with this part of the experiment is the rubber's ability to dampen the system by the experience of shear stress response to uniaxial stress. The stiffness value needs to be correlated with the rubber elements, by simulating the stiffness for the rubber elements isolated. While the damping coefficient is defined as a dashpot element since the acquirable Abaqus package does not include the possibility to run steady state analysis with smoothed particle hydrodynamic

part.

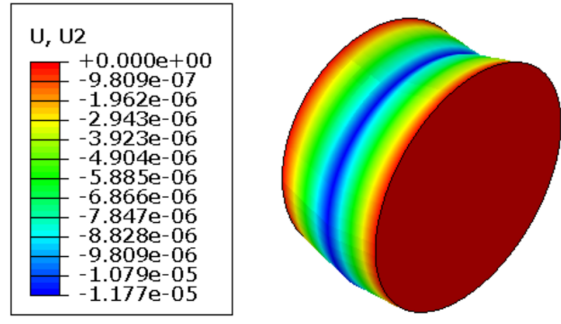


Figure 38: Static deflection analysis of rubber element.

Both rubber elements are considered to contribute to the  $k_2$  value in the Matlab code. The shear stiffness of the rubber elements is determined using the same procedure described in subsection 5.2. Before defining the elastic properties of the rubber material, a static analysis is performed to calculate the shear modulus of the rubber elements. Hooke's law,  $k = F/x$ , is employed to calculate the stiffness ( $k_2$ ). Figure 38 illustrates that a deflection of  $x = 1.177 \times 10^{-5}$  m with a force of  $F = 1.0$  N results in stiffness of  $k_2 = 85.0 \times 10^3$  N/m, which is approximately equal to the optimized stiffness obtained in Matlab. This stiffness requires Young's modulus of  $E = 2.0$  MPa, which is equal to the shear modulus  $G = 0.69$  MPa.

Another important parameter to consider is the Rayleigh damping data, which is defined in the steady-state dynamic step under the "damping" section. The eigenvalues obtained from a frequency analysis are presented in Figure 39. In this simulation, an assumption is made that only the tool body, without the attached damping system, contributes to the eigenvalues. Mode 1 exhibits a frequency of 199.2 Hz, while mode 2 corresponds to 1153.4 Hz.

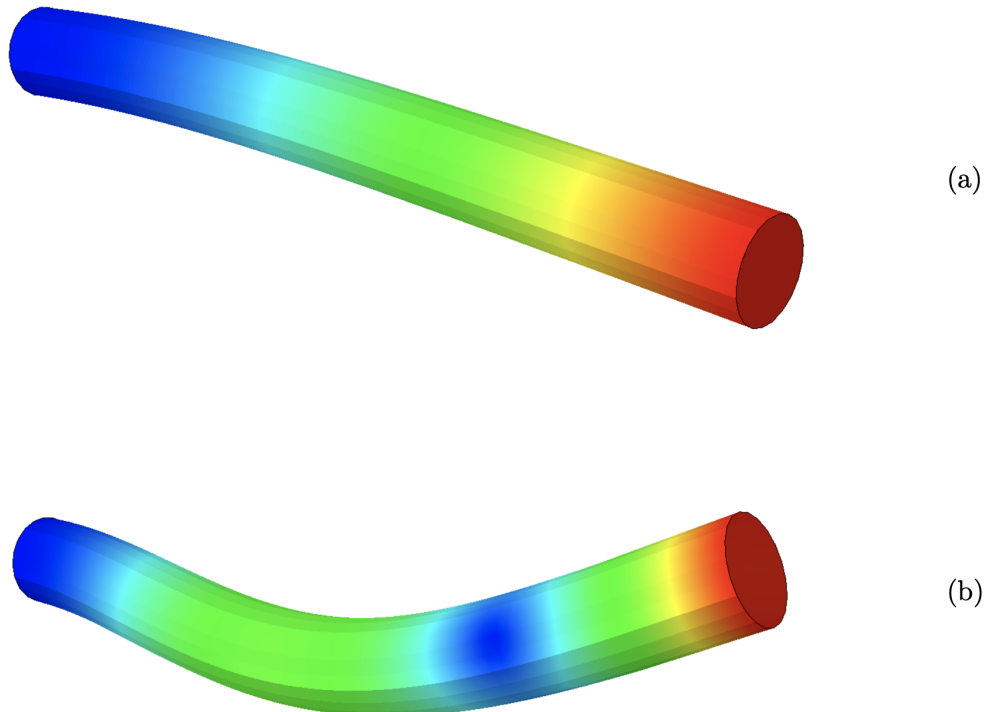


Figure 39: (a); Mode 1. (b); Mode 2.

The Rayleigh coefficients can be calculated using Equation (6), as previously presented. The damping ratio is determined from the frequency response function, illustrated in Figure 40, utilizing Equation (7). In this case, the natural frequency ( $f_n$ ) is found to be 199 Hz, corresponding to an amplitude peak of  $A_{max} = 4.072 \times 10^{-5}$  m. The frequencies at which  $A_{max}/\sqrt{2}$  occur are  $f_1 = 197$  Hz and  $f_2 = 201$  Hz. By calculating the damping ratio to  $\xi = 0.01$ , the resulting Rayleigh coefficients are determined to be  $\alpha = 0.02$  and  $\beta = 0.000015$ , which are applicable to all modes.

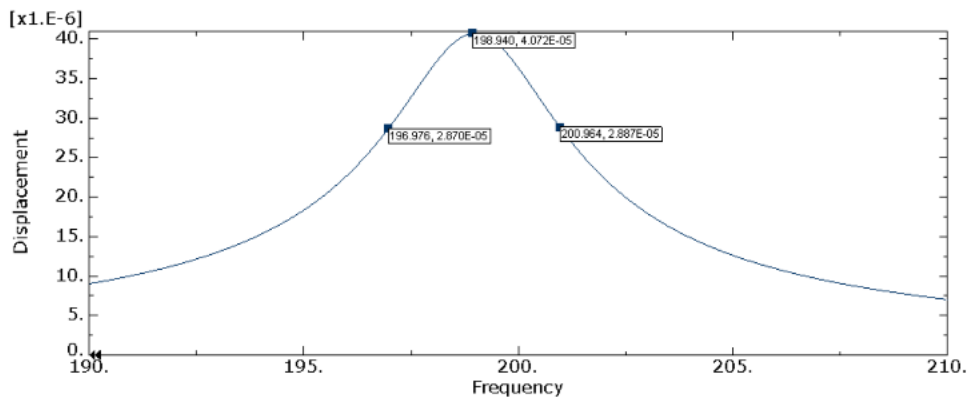


Figure 40: Frequency response function of the tool body.

The final parameter is the dashpot element, which is characterized by the optimized damping coefficient obtained through Matlab. The procedure involves connecting the moving mass to the tool body, as previously described, and defining the dashpot element with the optimized damping coefficient while leaving the spring undefined. The optimized FRF from Matlab and the FRF from Abaqus with equal  $k_2$  and  $c_2$  values yield two plots, as shown in Figure 41. Plot (b) shows a small tendency towards exhibiting two peaks, although it falls short of achieving the desired optimal damping when compared to the analytical FRF. On the other hand, plot (a) displays two equally amplified peaks, indicating the presence of an optimized FRF for the specific tool being studied. However, the amplitude in plot (b) significantly deviates from the desirable amplitude in plot (a).

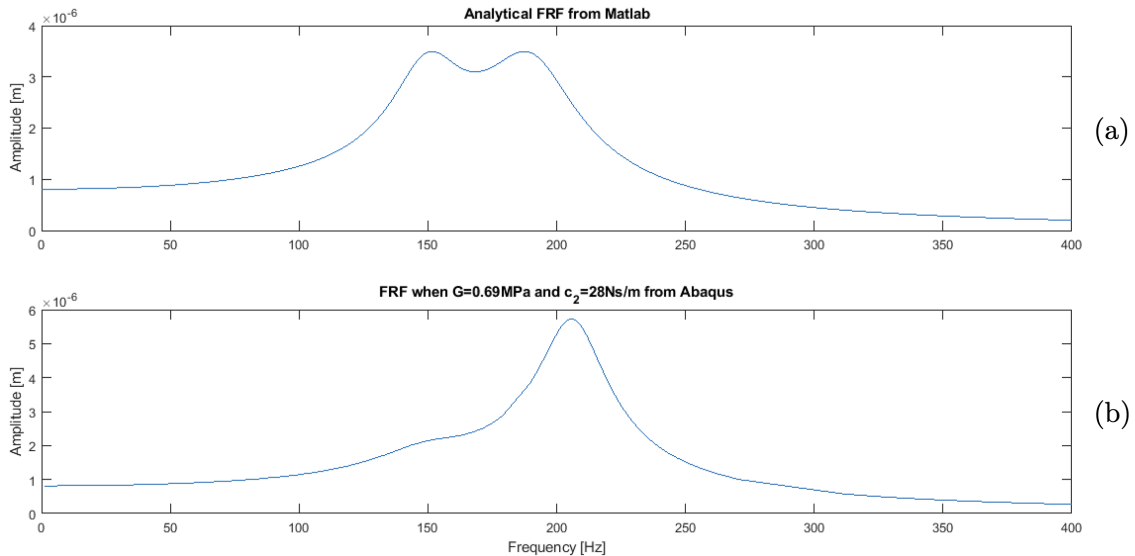


Figure 41: Frequency response function. (a); Analytical FRF of a two-mass system from Matlab. (b); FRF with rubber and dashpot values from Matlab inserted in Abaqus.

Further adjustments are required for Young's modulus of the rubber elements, which influence the stiffness and shear modulus. Figure 41 (b) reveals that an increased shear modulus is necessary, as experimented in subsection 4.1, when the right peak is larger than the left peak, the two peaks



will in this scenario equalize when increasing the stiffness. By slightly increasing Young's modulus to 2.67 MPa, a shear modulus of 0.92 MPa was obtained.

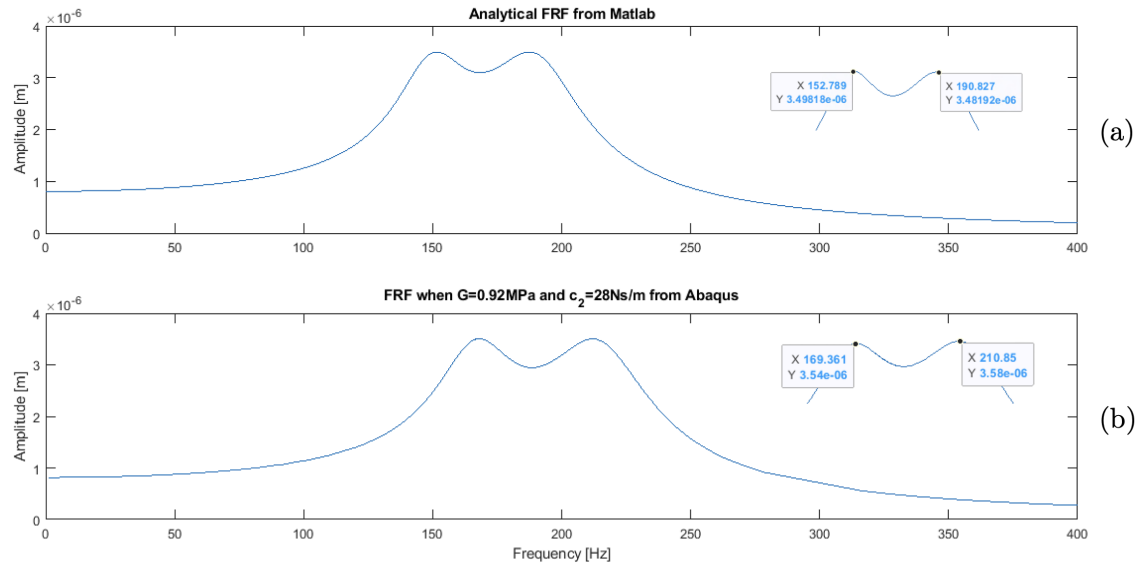


Figure 42: Frequency response function. (a); Analytical FRF of a two-mass system from Matlab. (b); FRF with adjusted shear modulus value inserted in Abaqus.

This new shear modulus results in an optimized FRF shown in Figure 42 (b). With the updated stiffness value of  $k_2 = 108.0 \times 10^3$  N/m, the two plots demonstrate a notable correlation, particularly in terms of their amplitude of  $3.5 \times 10^{-6}$  m. Both plots exhibit an FRF with two equalized peaks, which are observed at approximately the same frequencies, specifically around 150 – 170 Hz and 190 – 210 Hz. It is also noteworthy that the initial amplitude corresponds between the two models.

To get a better visual understanding of the model, a YouTube link is available here: [Click to watch video](#).

## 6.2 A Fluid-Affected Mass Subjected to Periodic Force

The Silent Tool incorporates a damping system consisting of a high-density cylinder between two rubber elements and surrounded by a viscous fluid. When the tool is in operation, the damping mass moves in various directions. Consequently, it is of interest to investigate the behavior of the fluid surrounding a cylindrical object subjected to a periodic force, in comparison to a dashpot element.

To conduct this study, an assembly model is created, isolating the damping system as illustrated in Figure 43, while excluding the rest of the tool body. The surrounding cylinder is fixed, and the cylindrical mass is centered and capable of movement along the  $y$ -axis. It is attached to each rubber element, utilizing the same dimensions as described in the previous subsection.

A general contact interaction is defined between the fluid and the solid components. As for the moving mass, a coupling constraint is positioned with a control point at the center of the mass. The defined mesh for the rubber elements is similar to the mesh used in earlier analyses including the rubber elements. As for the oil, a solid part is converted to 20 000 particles acting like a viscous fluid with a defined viscosity and density presented initially in this section.

The result will consist of three different setups, compared to the periodic amplitude representing the applied force. The only parameter varying is the viscous damping, where one model has particles, one has a dashpot element and the last one has neither fluid or dashpot. This is to compare how the periodic force will work differently in the three models.

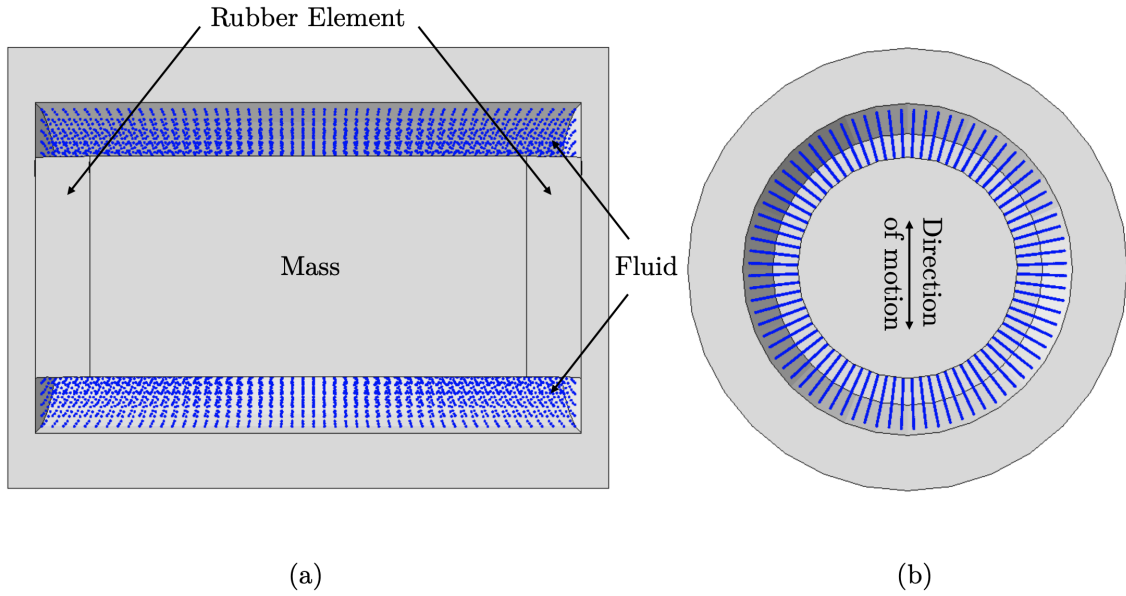


Figure 43: A view-cut of the model. (a); View of XY-plane. (b); View of XZ-plane

To simulate how the mass's motion is reacting at certain frequencies, the most suitable simulation method would be to perform a steady-state dynamic analysis. Since this is not attainable combined with an SPH part in the model, a force is applied with a given amplitude instead. With a specified periodic amplitude, it provides the possibility to examine the motion of the moving mass compared with the periodic force acting on the mass. The defined force is constant, while the circular frequency of the periodic amplitude varies. This means that the force acting on the moving mass is not constant, when the sinus curve peaks, it equals the defined load working in either positive or negative  $y$ -direction. This is to observe if there is any difference in the delay of motion compared to the force amplitude. The mass is situated at the center of the cylinder, and starting the mass from its equilibrium state ensures that it returns to the center after completing one wavelength. Hence, the choice of a sinusoidal curve is justified by considering the initial conditions.

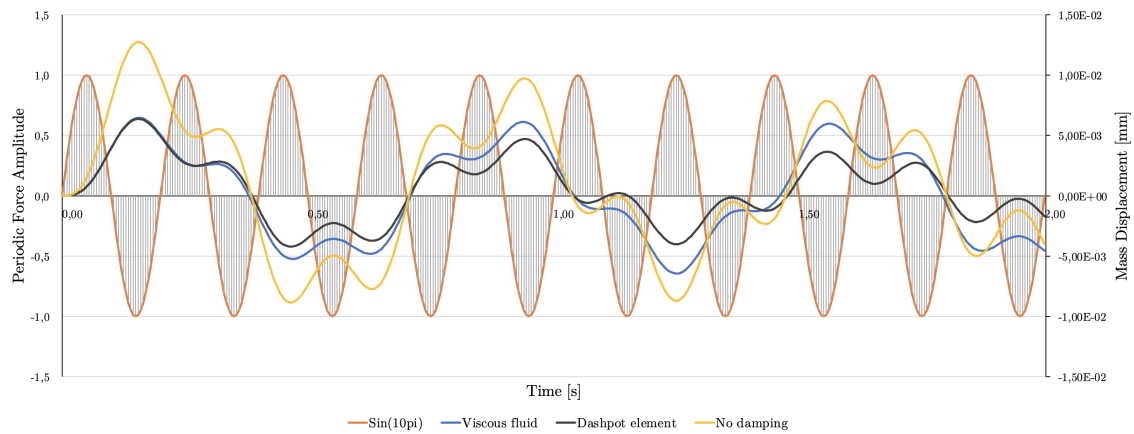


Figure 44: Applied periodic force ( $\sin(10\pi)$ ) compared with the displacement of the mass

Figure 44 illustrates a comparison among three models under an applied periodic sinusoidal curve with a frequency of 5.0 Hz. The orange line represents the periodic curve subjected to an applied force of 1.0 N, which is analyzed using all three models. The yellow line corresponds to the model with the largest displacement, indicating the least effect of damping, which is natural due to its missing viscous damping. In contrast, the model incorporating viscous damping exhibits a damping effect, resulting in minor deviations. The dashpot model (black line) is assigned a damping

---

coefficient of 100.0 Ns/m to assess its deflection in comparison to the fluid model (blue line).

All three models exhibit a consistent motion pattern, and it is evident that the presence of viscous fluid leads to a damping effect. The locations of the amplitudes are similar, confirming the comparable behavior of all three models. The most significant difference in amplitude is observed in the first wavelength. If the mass had not been connected to the rubber elements, this difference would have persisted for a longer duration.

The observed delay contributes to the non-uniform periodic motion of the mass. The sinusoidal curve is advancing at a faster rate than the moving mass can keep up with under the given conditions.

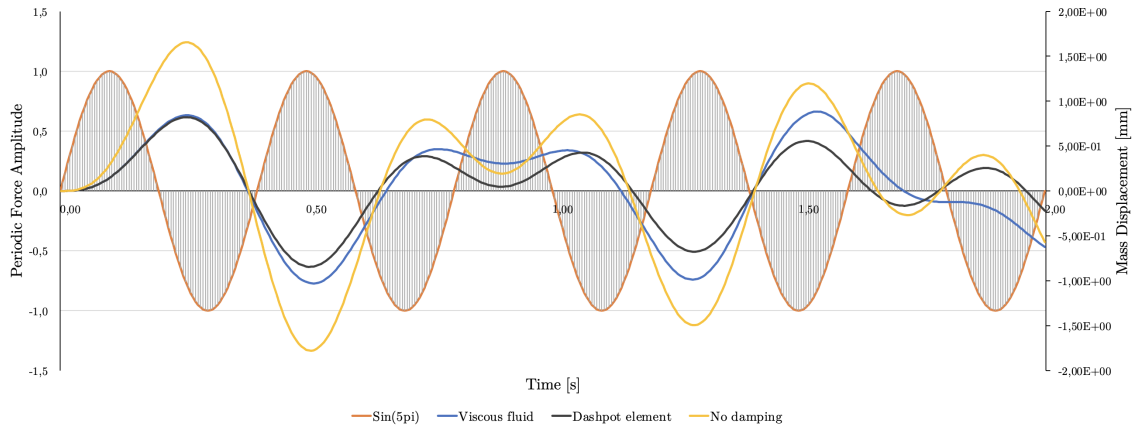


Figure 45: Applied periodic force ( $\sin(5\pi)$ ) compared with the displacement of the mass

The corresponding trend is seen in Figure 45. In this particular scenario, the force is elevated to 50.0 N with a periodic sinusoidal curve of 2.5 Hz. The purpose was to investigate the ability of the moving mass to synchronize with the periodic force. It is noteworthy that both figures provide some evidence regarding the damping phenomenon during the simulated two-second period, as indicated by the gradual decrease in maximum displacement across all three models.

To get a better visual understanding of the model, a YouTube link is available here: [Click to watch video](#)

---

## 7 Discussion

The study shows that Abaqus is a suitable tool for reproducing a simplified optimized boring bar that includes rubber elements and a dashpot element. However, when comparing the theoretical 2DOF model with the Abaqus-designed model, there are several factors and parameters that can contribute to potential errors and faults in the FRF comparison. This section discusses some of the potential sources of error.

In the case of fluid simulations, there is some uncertainty in the results due to the accuracy of SPH analysis in Abaqus, which can be influenced by various factors and parameters. This section provides an elaboration on some key factors that can introduce errors and faults in SPH analyses. Despite these considerations, the fluid simulations did demonstrate a visible damping effect.

### 7.1 Assessment of Shear Stiffness

The results of the study confirmed the validity of the rubber element using various simulation methods in Abaqus. By calculating shear stiffness and simulating Rayleigh damping coefficients, it becomes possible to explore geometrical modifications of the rubber elements for optimization. The shear stiffness was investigated by simulating multiple rubber elements analyses with varying the rubber's Young's modulus, confirming a linear relationship between shear stiffness and the applied Young's modulus. However, before making such modifications, a more realistic and complex model needs to be developed. This model should be compared to an actual boring bar to identify differences and areas for improvement. It is important to note that this thesis only compared a theoretical model to an Abaqus-designed model, but the underlying principles still apply.

Several factors may contribute to the need for adjustments compared to the optimal FRF obtained in Matlab. One possible factor is the placement of the entire damping system in the Abaqus model. The Matlab code for the theoretical two-mass system is based on the idea that the damping system is located at the very end of the simplified boring bar. Consequently, the equivalent modal mass calculated in Abaqus may not correspond to the theoretical equivalent modal mass used in Matlab. When reducing the input of the equivalent modal mass in Matlab, the left amplitude peak becomes lower compared to the right amplitude peak. This adjustment leads to an FRF that shows some resemblance to the initial attempt of the simplified boring bar in Abaqus. However, it is not as simple as just changing the equivalent modal mass, as doing so affects the viscous damping coefficient due to the formula used for its calculation. By theoretically decreasing the equivalent modal mass and incorporating the stiffness value obtained from the optimized stiffness in Abaqus, it is possible to achieve an FRF in Matlab that closely resembles the FRF obtained in Abaqus, with a similarly applied stiffness and damping coefficient. This adjustment also enables the entire FRF to shift to the right, resulting in more similar natural frequencies compared to the simplified boring bar in Abaqus.

The accuracy of material properties incorporated into the Abaqus model plays a crucial role in the reliability of the FRF comparison. The theoretical model consists of simplified assumptions about material behavior, overlooking factors such as material nonlinearities and viscoelasticity that can impact the system's response. In contrast, Abaqus allows for the inclusion of more precise material properties obtained from experimental data or detailed material models. By utilizing these accurate material properties, the Abaqus model enhances the accuracy of the FRF comparison.

As for the approach to finding Rayleigh damping coefficients, the half-power bandwidth method confirms a certain validity to the damping ratio which resulted in a dampening effect. Hence this observation, the differences observed in the resulting FRFs can be caused due to incorrect Rayleigh damping coefficients. Adjusting the coefficient in proportion to the system's mass ( $\alpha$ ) can lead to changes in the FRF, including a decrease in the amplitude on the right side and an increase on the left side, resulting in a higher maximum amplitude. Conversely, increasing the coefficient in proportion to the system's stiffness ( $\beta$ ) can cause the two peaks in the FRF to approach each other, leading to uneven peaks. If the coefficient becomes too large, it may ultimately merge the peaks into a single peak, which deviates from desired optimized two equalized peaks. Hence, even small

---

errors in these coefficients can lead to undesired changes and potential flaws in the resulting FRF. Therefore, it is crucial to carefully determine and validate these coefficients to ensure accurate FRF predictions. One approach to solve this could involve determining the Rayleigh damping coefficients experimentally for both the tool body and the rubber elements. A possible error in the combined simulation is the assumed common set of damping coefficients utilized for the entire model and not two different sets of coefficients disturbed to the rubber elements and the tool body. To validate this result, an experimental impact test using appropriate vibration measurement equipment should be performed.

The simplified boring bar required partitioning using finite elements, and the choice of meshing and element types could have influenced the FRF since it can affect the accuracy of the result. The odds of inadequate mesh refinement or inappropriate element types creating errors in the FRF are reduced due to regular testing of the mesh.

It is important to note that the results obtained are not necessarily intended to replicate the behavior of a realistic tool damper. This is primarily due to assumptions made regarding material properties and simplifications in the model. These decisions were made to ensure a high level of similarity between the Abaqus model and the theoretical model, allowing for a more precise comparison of the spring and damping coefficients. Future work should involve developing a more detailed model and comparing it to an existing Silent Tool. Defining an amplitude reflecting the realistic cutting force could have been interesting to apply to the simplified boring bar. This would help create an even more realistic frequency response function due to the assumed constant cutting force in this thesis. Also, comparing the detailed Abaqus model with experimental data can help identify and address any errors or discrepancies, such as incorrect load conditions, improper location of the cutting force, or inadequate boundary conditions.

## 7.2 Evaluation of Fluid Simulations

Some factors causing the small difference between the translatory damping coefficient obtained from the SPH analyses compared to the iterative analytical approach are discussed here. The terminal velocity of the mobile cylinder was found to be lower than the terminal velocity calculated analytically, suggesting the presence of some error. The most probable cause of the error is the relative velocity. The velocity graph presented only considers the cylinder's velocity and does not account for the particles moving in the opposite direction, resulting in a higher relative velocity. The relative velocity is a more suitable velocity that should have been used for the calculation of the translatory damping coefficient. When tracking the velocity of a specific particle moving alongside the cylinder in the opposite direction, a higher relative velocity is observed. This error could have occurred because the gradient of the relative velocity between the moving surface and the fixed one is assumed to work in the same direction as the mobile cylinder. To reduce this error, one option is to increase the gap between the moving cylinder and the shell cylinder, making the particles pushed by the moving cylinder travel more scattered and not as a concentrated flow in the opposite direction.

The comparison between the two rotary damping coefficients did not match, possibly due to flaws in the simulation setup and limited access to a sufficient number of computing cores, which hindered the achievement of optimal results. The main difference between the model geometry is that the "side-walls" in the Abaqus model are exposed as a friction surface, and could provide a higher fluid resistance, but this error alone seems unlikely to cause the large difference. The limited number of converted particles, constrained by time and computational limitations, may have contributed to the observed differences in the rotary damping coefficients. The absence of a fixed mesh introduces challenges in capturing complex geometries, interfaces, and contact interactions accurately. The method used to determine the rotary damping coefficients is also a subject for discussion, particularly regarding its comparability. The theoretical approach focuses on examining the gradient of the relative velocity between the rotary shaft and the radial bearing. Obtaining this information in Abaqus was challenging due to the computational cost.

The resulting viscous damping effect on the mass when subjected to a periodic force does not align with a realistic operational frequency range. This is because the Silent Tool typically operates

---

at higher frequencies. The purpose of using these low frequencies was to visually highlight the differences among the three models. By simulating a simplified boring bar with a periodic force with a 200 Hz frequency, it became challenging to observe the distinctions due to the rapid and short-lived periodic motions. The objective of the simulation was to investigate whether the fluid had any damping effect when a low-frequency force was applied to the mass. While the results indicate the presence of viscous damping, further validation is necessary due to the limited outcomes obtained from the analysis.

One common source of error in SPH simulations arises from the substantial computational resources required. Inadequate hardware configurations, characterized by limitations in processing power and memory capacity, can significantly impact the accuracy and efficiency of the analysis. To address and minimize these sources of error and faults in SPH analyses, several steps can be taken. For example, conducting mesh convergence studies using more robust hardware configurations can help ensure reliable results. By refining the mesh and evaluating the convergence of the simulation, the accuracy of the analysis can be improved. Additionally, it is crucial to validate the simulation results against experimental data. Comparing the simulated outcomes with real-world measurements allows for verification of the accuracy and reliability of the SPH analysis. In dynamic analyses, the simulation time is divided into increments to discretize the process. However, if incrementation strategies are not necessarily accurately employed throughout this thesis it may have been leading to unstable or inaccurate simulations of fluid models. It is also important to acknowledge that mass scaling, may have introduced some errors into the fluid simulations. The purpose of using mass scaling is to reduce computational time, but it was difficult to validate the correct use of this feature. It is important to use mass scaling with caution and validate the results against experimental data to ensure the accuracy and reliability of the simulation.

---

## 8 Conclusion

In conclusion, the objective of this study was to validate the accuracy and reliability of Abaqus in producing dependable results. By confirming the capabilities of Abaqus, Sandvik Coromant can effectively make adjustments to tool designs or material properties with greater efficiency. Through various analyses and comparisons, it was demonstrated that Abaqus can provide reliable insights into tool performance, enabling informed decision-making in design optimization. The utilization of advanced modeling techniques, such as dynamic analyses and fluid-structure interaction, further enhanced the understanding of complex tool behavior. Overall, the validation of Abaqus as a tool for engineering analysis empowers Sandvik Coromant to continuously enhance tool designs and ensure optimal performance in real-world applications.

The comparison between the fluid analysis using SPH in Abaqus and the analytical calculation revealed interesting findings. The analyses considered translatory and rotary damping coefficients. The translatory damping coefficient obtained from Abaqus showed similarities when compared to the analytical approach, providing confidence in its accuracy. However, there was a noticeable disparity in the results of the rotary damping coefficient, raising concerns about its accuracy. This discrepancy could potentially be attributed to various sources of error, which need to be further investigated and addressed to improve the reliability of the rotary damping coefficient in SPH analyses.

After conducting several analyses of the spring/dashpot element in Abaqus, it can be concluded that it is highly reliable, as it demonstrates strong similarities to analytical methods. The comparison of the FRFs between the simplified two-mass systems clearly shows a high degree of correspondence in both frequencies and amplitudes. This knowledge opens up possibilities for further advancements in the model, such as simulating different rubber element geometries with an applied dashpot element to represent the damping coefficient. By replacing the fluid with a dashpot element, significant computational time can be saved while still capturing the essential damping behavior. This approach allows for more efficient exploration of design variations and optimization strategies in a timely manner.

Further experimentation and testing are recommended to compare the proper damping behavior of the rubber material using Rayleigh damping coefficients. However, the damping coefficients applied to the model resulted in a damping effect observed during impact analysis. By geometric testing of the rubber elements, the half-bandwidth method can be used as a temporary solution to calculate the damping ratio and determine the appropriate Rayleigh damping coefficients. This approach provides a practical way to capture the desired damping behavior and improve the accuracy of the simulation results.

The combined simulations provided promising results, with the damping behavior of the simplified boring bar corresponding to the analytical predictions. By incorporating proper shear stiffness for the rubber elements, applying the dashpot element with confidence, and using Rayleigh damping coefficients, the simulated two-mass system achieved optimized damping behavior. However, certain discrepancies between the Abaqus model and the analytical predictions were observed due to geometrical differences and assumptions made. The presence of viscous fluid in the combined SPH model contributed to damping, but accurately assessing its real-world correspondence remains challenging. These findings highlight the complexity of the simulated boring bar, suggesting further refinement and investigation.

### 8.1 Further Work

Further validation is strongly recommended to accurately evaluate the parameters required for creating an FRF for a more detailed boring bar. Additionally, conducting further experiments to simulate a damping coefficient between the mass and the fluid in the dampening viscous fluid model would be beneficial.

The simplified boring bar can be modeled with accurate geometry, resulting in a more realistic FRF of the Silent Tool. The assumed weight of the damping mass has an impact on the FRF,

---

increasing the weight leads to different optimized stiffness and damping coefficients. Currently, the mass is constrained to deflect only along the  $y$ -axis, which is an unrealistic assumption since the boring bar will experience deflection in all directions during operation. There is also recommended to further explore the periodic force amplitude, applied as a more realistic cutting force to the tool. This method allows simulations of SPH analyses. Additionally, it may be valuable to try out Abaqus' "gasket thickness behavior" material definition, as well as the "gasket transverse shear elastic" material behavior, which can save the user some time. Providing an input box to define the shear stiffness could be a helpful addition.

In terms of SPH analysis, accessing a greater number of cores is essential to simulate large-scale SPH analyses due to the significant time requirements involved. By increasing the number of particles and extending the duration of the time step, the damping behavior can be further explored, leading to more accurate results. It is worth considering the inclusion of fluid temperature since it has an impact on dynamic viscosity. The viscous properties of the fluid decrease rapidly as temperature increases, which can result in a varying damping coefficient influenced by the frequency and duration of the motion.



---

## Bibliography

- [1] I. RheoSense. ‘What are the differences between dynamic and kinematic viscosities?’ (), [Online]. Available: <https://blog.rheosense.com/what-are-the-differences-between-dynamic-and-kinematic-viscosities> (visited on 21st Mar. 2023).
- [2] S. Pump. ‘Know your pump’s viscosity limit’. (), [Online]. Available: <https://summitpump.com/know-your-pumps-viscosity-limit/> (visited on 17th Feb. 2023).
- [3] E. Britannica. ‘Viscosity’. (), [Online]. Available: <https://www.britannica.com/science/viscosity#:~:text=What%20is%20the%20unit%20of,pascal%2Dsecond%20in%20SI%20units> (visited on 30th Apr. 2023).
- [4] N. Lobontiu, *System Dynamics for Engineering Students*. Academic Press, 2018.
- [5] N. Lobontiu, *System Dynamics for Engineering Students*. Academic Press, 2018.
- [6] E. Britannica. ‘Terminal velocity’. (), [Online]. Available: <https://www.britannica.com/science/terminal-velocity> (visited on 2nd May 2023).
- [7] N. H. NASA. ‘Terminal velocity interactive’. (), [Online]. Available: <https://www1.grc.nasa.gov/beginners-guide-to-aeronautics/termvel/#drag> (visited on 25th Apr. 2023).
- [8] Unknown. ‘Terminal velocity’. (), [Online]. Available: [https://en.wikipedia.org/wiki/Terminal\\_velocity](https://en.wikipedia.org/wiki/Terminal_velocity) (visited on 25th Apr. 2023).
- [9] Simscale. ‘What is reynolds number?’ (), [Online]. Available: <https://www.simscale.com/docs/simwiki/numerics-background/what-is-the-reynolds-number/> (visited on 6th Mar. 2023).
- [10] A. K. Dey. ‘Definition of reynold’s number’. (), [Online]. Available: <https://whatispiping.com/reynolds-number/> (visited on 7th Mar. 2023).
- [11] E. W. Weisstein. ‘Fluid mechanics, cylinder drag’. (), [Online]. Available: <https://scienceworld.wolfram.com/physics/CylinderDrag.html> (visited on 6th Mar. 2023).
- [12] Unknown. ‘Flow around immersed bodies’. (), [Online]. Available: [https://www.uobabylon.edu.iq/eprints/paper\\_2\\_2327\\_1369.pdf](https://www.uobabylon.edu.iq/eprints/paper_2_2327_1369.pdf) (visited on 7th Mar. 2023).
- [13] D. Systèmes. ‘Fluid structure interaction analysis with abaqus and fluent’. (), [Online]. Available: <https://www.3ds.com/fileadmin/PRODUCTS/SIMULIA/PDF/tech-briefs/Cross-Fluid-Structure-Interaction-with-Abaqus-FLUENT-05.pdf?links=false> (visited on 27th Apr. 2023).
- [14] F. Codes. ‘What is fluid-structure interaction and how can you simulate it?’ (), [Online]. Available: <https://fluidcodes.com/news/what-is-fluid-structure-interaction-and-how-can-you-simulate-it/> (visited on 14th Feb. 2023).
- [15] D. systemes. ‘Introduction to abaqus/cfd’. (), [Online]. Available: <https://imechanica.org/files/CFD.pdf> (visited on 14th Apr. 2023).
- [16] A. U. Guide. ‘Defining a fluid-structure co-simulation interaction’. (), [Online]. Available: <http://130.149.89.49:2080/v6.13/books/usi/default.htm?startat=pt03ch15s13h1b13.html> (visited on 15th Feb. 2023).
- [17] A. U. Guide. ‘Smoothed particle hydrodynamics’. (), [Online]. Available: <http://130.149.89.49:2080/v6.14/books/usb/default.htm?startat=pt04ch15s02aus95.html> (visited on 21st Mar. 2023).
- [18] D. Systèmes. ‘Smoothed particle hydrodynamics’. (), [Online]. Available: <https://docs.software.vt.edu/abaqusv2022/English/SIMACAEANLRefMap/simaanl-c-sphanalysis.htm> (visited on 27th Apr. 2023).
- [19] A. A. U. Guide. ‘Dynamic analysis procedures: Overview’. (), [Online]. Available: <https://classes.engineering.wustl.edu/2009/spring/mase5513/abaqus/docs/v6.6/books/usb/default.htm?startat=pt03ch06s03abo06.html> (visited on 4th Mar. 2023).
- [20] E. O. C. A. Group. ‘Abaqus/standard or abaqus/explicit’. (), [Online]. Available: <https://caeassistant.com/blog/abaqus-standard-or-abaqus-explicit/> (visited on 3rd Mar. 2023).
- [21] Özgün. ‘What is explicit dynamics in ansys?’ (), [Online]. Available: <https://www.mechead.com/what-is-explicit-dynamics-in-ansys/> (visited on 5th Mar. 2023).

- 
- [22] Y. ÇAPAR. ‘Implicit vs explicit approach in fem’. (), [Online]. Available: <https://yasincapar.com/implicit-vs-explicit-approach-in-fem/> (visited on 4th Mar. 2023).
- [23] S. N. R. Center. ‘Mass scaling in abaqus’. (), [Online]. Available: <https://numericalarchive.com/2022/07/21/abaqus-mass-scaling/> (visited on 10th May 2023).
- [24] A. A. U. Guide. ‘Mass scaling’. (), [Online]. Available: <https://classes.engineering.wustl.edu/2009/spring/mase5513/abaqus/docs/v6.6/books/usb/default.htm?startat=pt04ch11s07aus63.html> (visited on 3rd Mar. 2023).
- [25] A. A. U. Guide. ‘26.2.1 dashpots’. (), [Online]. Available: <https://classes.engineering.wustl.edu/2009/spring/mase5513/abaqus/docs/v6.6/books/usb/default.htm?startat=pt06ch26s02alm36.html> (visited on 10th Mar. 2023).
- [26] A. A. U. Guide. ‘26.1.1 springs’. (), [Online]. Available: <https://classes.engineering.wustl.edu/2009/spring/mase5513/abaqus/docs/v6.6/books/usb/default.htm?startat=pt06ch26s02alm36.html> (visited on 10th Mar. 2023).
- [27] E. O. C. A. Group. ‘Material damping in abaqus’. (), [Online]. Available: <https://caeassistant.com/blog/material-damping-in-abaqus/> (visited on 10th Mar. 2023).
- [28] A. A. U. Guide. ‘5.1.2 \*amplitude’. (), [Online]. Available: <https://classes.engineering.wustl.edu/2009/spring/mase5513/abaqus/docs/v6.6/books/ver/default.htm?startat=ch05s01abv274.html> (visited on 14th May 2023).
- [29] D. Systèmes. ‘Rayleigh damping’. (), [Online]. Available: [https://help.solidworks.com/2016/english/solidworks/cworks/c\\_rayleigh\\_damping.htm](https://help.solidworks.com/2016/english/solidworks/cworks/c_rayleigh_damping.htm) (visited on 10th Apr. 2023).
- [30] Orcaflex. ‘Rayleigh damping’. (), [Online]. Available: <https://www.orcina.com/webhelp/OrcaFlex/Content/html/Rayleighdamping.htm> (visited on 25th Mar. 2023).
- [31] G. Giraldo. ‘How to compute the coefficients for rayleigh damping?’ (), [Online]. Available: <https://www.simscale.com/knowledge-base/rayleigh-damping-coefficients/> (visited on 5th Mar. 2023).
- [32] I. Integrated Systems Research. ‘Half power damping estimations’. (), [Online]. Available: [https://www.isrtechnical.com/media/tech-briefs/estimating\\_damping\\_values.pdf](https://www.isrtechnical.com/media/tech-briefs/estimating_damping_values.pdf) (visited on 9th Apr. 2023).

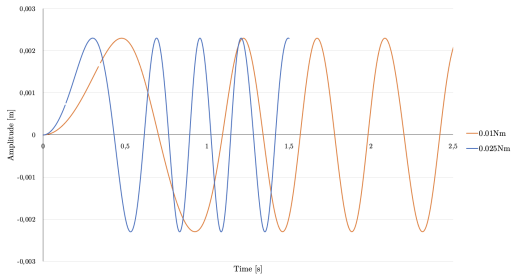
# Appendix

## A Rotary Damping Data

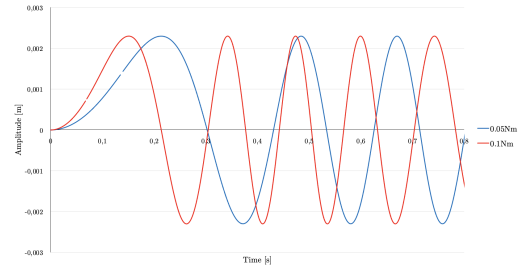
This is an overview of the calculations related to the rotary damping SPH model. It is important to note that these calculations are based on the assumption of a linear damping model. Rotary motion with different applied torque, with stabilized wavelengths, is illustrated in Figure 46.

Table 4: Rotary model results

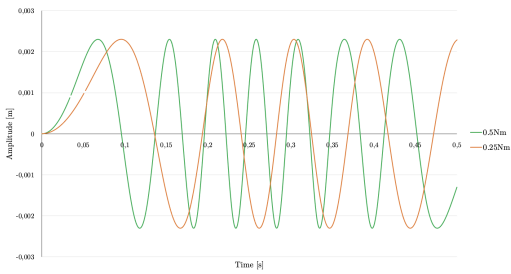
Torque, $m_d$ [Nm]	Wavelength, $\lambda$ [s]	Tangential velocity, $v$ [m/s]	Angular velocity, $\omega$ [rad/s]	Damping coefficient, $c_r$ [Nms/rad]
0.01	0.425	0.0318	14.8	$6.80 \times 10^{-4}$
0.025	0.265	0.0510	23.7	$1.05 \times 10^{-3}$
0.05	0.175	0.0772	35.9	$1.39 \times 10^{-3}$
0.10	0.135	0.1001	46.5	$2.15 \times 10^{-3}$
0.25	0.092	0.1466	68.2	$3.67 \times 10^{-3}$
0.50	0.064	0.2121	98.6	$5.07 \times 10^{-3}$
0.75	0.052	0.2616	121.7	$6.16 \times 10^{-3}$
1.00	0.045	0.3002	139.6	$7.16 \times 10^{-3}$



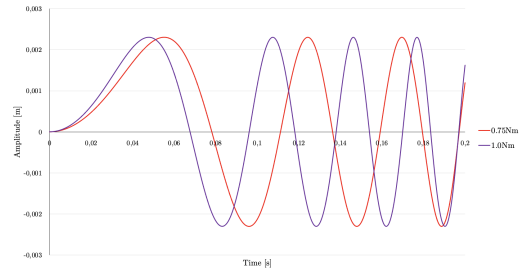
(a) 0.01 Nm and 0.025 Nm



(b) 0.05 Nm and 0.1 Nm



(c) 0.25 Nm and 0.5 Nm



(d) 0.75 Nm and 1.0 Nm

Figure 46: Rotary motion from SPH simulations

---

## B Abaqus Meshing Techniques

Various meshing methods were developed during the specialization project (TPK4540). One of the project's targets was to identify the most suitable mesh type for the model, which is utilized in this master's thesis. Mesh size analyses were performed whenever the model incorporated new geometries. The number of elements was increased iteratively until the resulting output reached a stable value, with the exception of the fluid. Due to computational limitations, the mesh size for the fluid analysis was constrained. The following figures illustrate the specific mesh type and size used.

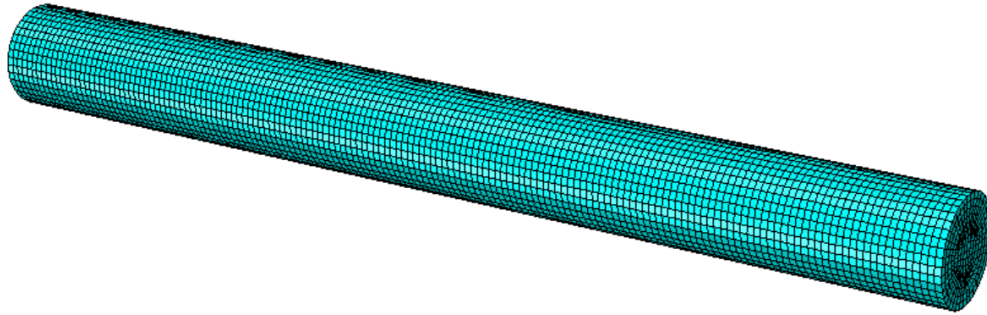


Figure 47: Linear standard 3D stress, 37 586 elements

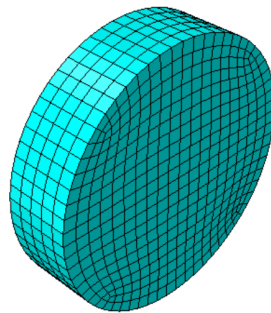


Figure 48: Linear standard 3D stress, 1 920 elements

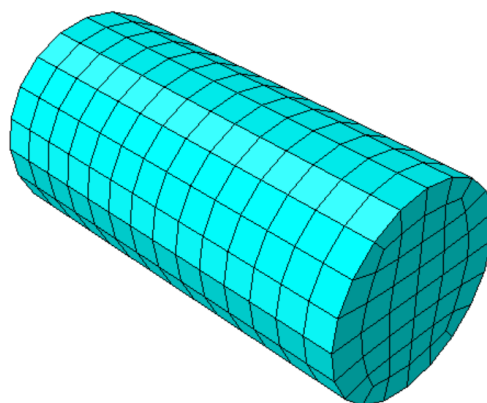


Figure 49: Linear standard 3D stress, 616 elements

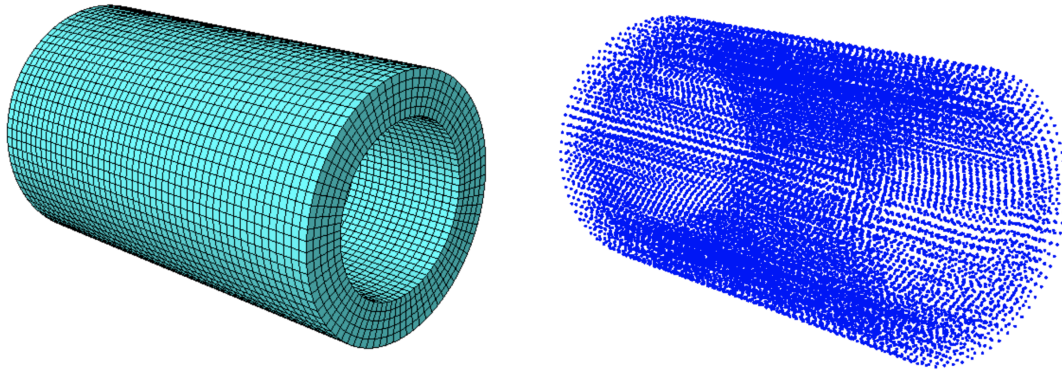


Figure 50: Linear explicit 3D stress, 20 000 elements/particles

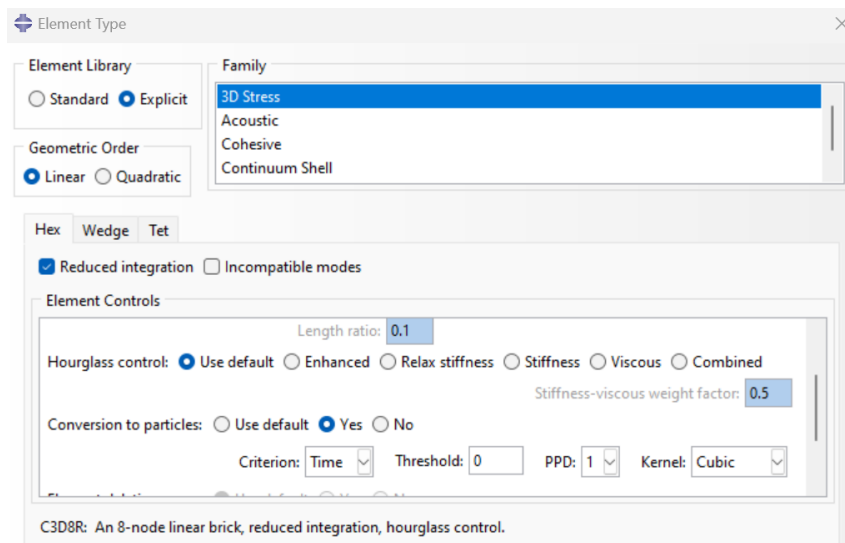


Figure 51: Fluid part conversion to particles

---

## C Optimal TMD Matlab Code

*%Using the MATLAB function fminsearch to find the values of k2 and c2 that will  
→ minimize the magnitude curve of the two-mass system*

```
function maxPoint = OptimalTMD(x)

m1 = 0.98; %[kg]
k1 = 1.24e6; %[N/m]
c1 = 44.2; %[Ns/m]
m2 = 0.08; %[kg]
k2 = x(1); %[N/m]
c2 = x(2); %[Ns/m]

w = [0:1:2500]; %[rad/s]

TF = (k2-m2*w.^2+1i*c2*w)./(-m1*m2*w.^4+...
    (m1*c2+c2*m2+c1*m2)*1j*w.^3+(k1*m2+k2*m2+m1*k2+c1*c2)*w.^2-...
    (k1*c2+c1*k2)*1j*w-k1*k2);

magnitude = abs(TF);

plot(w./(2*pi), magnitude)
pause(0.1)

maxPoint=max(magnitude);

end

%New file to call optimization function

clc
close all
clear all

% function call
figure
[opt, ~] = fminsearch(@OptimalTMD,[3e5 200]);
k2 = opt(1);
c2 = opt(2);
fprintf('The optimized stiffness is %d, and the optimized damping is  
→ %d\n',k2,c2);

% repeating problem one with new values
N = (k2-m2*w.^2+1i*c2*w)./(-m1*m2*w.^4+...
    (m1*c2+c2*m2+c1*m2)*1j*w.^3+(k1*m2+k2*m2+m1*k2+c1*c2)*w.^2-...
    (k1*c2+c1*k2)*1j*w-k1*k2);
amp = abs(N);

figure
plot(w./(2*pi), amp)
ylabel('Amplitude, m ')
xlabel('Frequency, Hz')

% maximum magnitude
[max_magnitude, max_frequency] = max(amp);
```

---

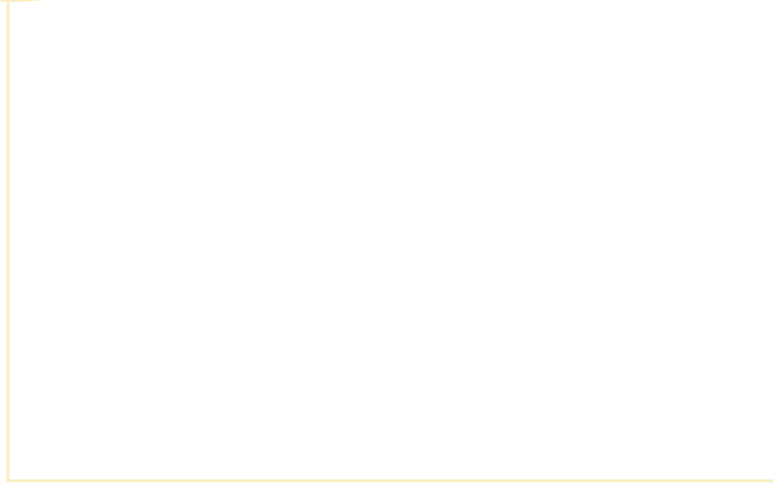
---

```
fprintf('Maximum magnitude of %d, at a frequency of %d with optimized k2 and  
→ c2\n',max_magnitude, max_frequency)
```

Output data from command window:

The optimized stiffness is 8.518987e+04, and the optimized damping is 2.861005e+01

*This code is sourced from the "Machining and Additive Manufacturing" course (TPK4440) at NTNU.*



 **NTNU**

Norwegian University of  
Science and Technology